

**ANTI-REFLECTIVE AND OPTICAL
TRANSPARENT COATINGS FOR THIN FILM
SOLAR CELLS AND GLASSES**

**A Thesis Submitted to
the Graduate School of Engineering and Sciences of İzmir Institute of
Technology
in Partial Fulfillment of the Requirements for the Degree of**

MASTER OF SCIENCE

in Energy Systems Engineering

**by
Shukrullo Kamolov**

**July 2020
İZMİR**

ACKNOWLEDGEMENT

First of all, I would like to thank my supervisor Prof. Dr. Lütfi ÖZYÜZER for his extensive support, encouragement and valuable time and experience, which patiently shared during this research, also for permanent care, moral support and valuable suggestions I am grateful to Prof. Dr. Gülnur AYGÜN.

Also, I would like to thank thesis committee members Prof. Dr. Gülden GÖKÇEN AKKURT and Asst. Prof. Özge SAĞLAM for their interest, sincerity, participation, and valuable comments.

I wish to thank my dear teacher Dr. Yasemin DEMİRHAN who gave information about my experimental studies, theoretical knowledge, and solutions. She helped to form my master's thesis and provided me with the support I needed.

I am grateful to TÜBİTAK 1512-2180410 project that supported me throughout my studies. This research also was partially supported by Teknoma Technological Materials Industrial and Trading Inc.

In addition, I appreciate of all group members Çağlar GEDİKSİZ, Merve EKMEKCİOĞLU, José Enrique MARTÍNEZ MEDİNA and other laboratory colleagues, who have always been with me with their productive supports.

Finally, more importantly, I would like to thank my dear family for all their support, understanding and encouragement in this period.

ABSTRACT

ANTI-REFLECTIVE AND OPTICAL TRANSPARENT COATINGS FOR THIN FILM SOLAR CELLS AND GLASSES

Antireflective coatings in some implementation necessary for the decreasing surface reflection, but in some applications also for increasing transmittance. Incident radiation on the surface of the optical material is divided into transmitted, reflected, scattered, and absorbed proportions, and the proportion of current energy that deployed among them is defined by RI (refraction indices).

Solar panels made from crystalline or polycrystalline silicon, but another type of solar panel is a thin-film solar panel. Thin-film technology has several advantages, such as low material consumption, which leads to cost savings to production, the ability to absorb diffused solar radiation, a relatively high efficiency (up to 20%), long service life (efficiency decreases by 10-15% of the initial efficiency). For all types of photovoltaic devices, energy loss is an important issue.

Single-layer and two-layer antireflection coatings with a low refractive index, coated and uncoated (SiO_2) thin-film with the sol-gel method were prepared and compared in terms of performance and continuity. The photocatalytic performance of (SiO_2) thin films in 1, 2, 3, 4, 5 and 24 hours was defined with methylene blue dye solution (20 mL) under UV source and was illuminated by it. The I-V characteristics curve of solar cells for small and large area was learned and increasing efficiency was observed. Adhesion tests in this study was applied by tape tests on substrates of glass.

As a result, the field tests of small and large area glasses coated solar panels were realized, the low reflectance and high efficiency were obtained.

ÖZET

İNCE FILM GÜNEŞ HÜCRELERİ VE CAMLAR İÇİN YANSITMASIZ VE OPTİK GEÇİRGEN KAPLAMALAR

Yansıtıcı kaplamalar bazı uygulamalarda yuzu yansıma azalan camlar için gerekli olmakla birlikte, bazı uygulamalarda geçirgenliği arttırmak için de gereklidir. Optik malzemenin yüzeyindeki radyasyon iletilen, yansıtılan, dağıtılan ve emilim oranlarına bölünür ve aralarında dağıtılan mevcut enerjinin oranı RI (kırılma indeksleri) ile tanımlanır.

Güneş panelleri kristal veya polikristalin silikondan yapılır, ancak başka bir güneş paneli tipi ise ince filmlili güneş panelidir. İnce film teknolojisinin düşük malzeme tüketimi, yayılan güneş radyasyonunu emme yeteneği, nispeten yüksek verimlilik (% 20'ye kadar) ve uzun hizmet ömrü (verimlilik, ilk verimliliğin% 10-15'i kadar azalır) gibi çeşitli avantajları vardır, bu nedenle ciddi bir maliyet tasarrufu sağlanmaktadır. Tüm fotovoltajik cihazlar için enerji kaybı önemli bir konudur.

Sol-jel yöntemi ile kaplanmış ve kaplanmamış (SiO_2) ince film, düşük kırılma indeksine sahip tek katmanlı ve iki kamala yansıma önleyici kaplamalar hairtails, performans ve süreklilik açısından karşılaştırılmıştır.

1, 2, 3, 4, 5 ve 24 saatteki SiO_2 ince filmlerinin fotokatalitik performansı, UV kaynağı altında aydınlatıldı ve metilen mavisi boya çözeltisi (20 mL) ile belirlendi. Küçük ve büyük alanlar için güneş pillerinin I-V karakteristik eğrisi öğrenildi ve verimliliğin arttığı gözlemlendi. Bu çalışmada yapışma testleri, cam yüzeyler üzerinde bant ile uygulanmıştır.

Sonuç olarak, küçük ve geniş boyutlu cam kaplamalı güneş panellerinin saha testleri gerçekleştirilmiş, düşük yansıma ve yüksek verim elde edilmiştir.

To my family...

TABLE OF CONTENTS

LIST OF FIGURES.....	viii
LIST OF TABLES	x
CHAPTER 1. INTRODUCTION	1
1.1. The Energy Power of Sun.....	1
1.2. Photovoltaic technology.....	2
1.3. Purpose of the Thesis.....	5
CHAPTER 2. THEORETICAL BACKGROUND	6
2.1. Antireflective Coatings	6
2.1.2. The Single Layer ARC	8
2.1.3. Double Layer ARC	9
2.1.4. The Multilayer ARC	10
2.2. Deposition Techniques of AR for Thin Films	11
2.2.1. Sol-gel Process	12
2.2.2. Dip-Coating method	13
2.2.3. Spray Coating Method	14
CHAPTER 3. EXPERIMENTAL PROCEDURE	16
3.1. Preparation of AR Solution	16
3.2. Fabrication of AR Thin Film	17
3.2.1. Small Area AR Coatings by Dip Coating Method	19
3.2.2. Large Area AR Coatings by Spraying-Coating Method	19
3.3. Optical Characterization of AR Surfaces	20
3.3.1. SEM Analysis	20
3.4. UV Spectrophotometer Measurements	21
3.5. Photocatalytic Degradation of Methylene Blue Dye Test	21
3.6. Adhesion Test of AR Coatings	25
3.7. Solar Radiation Measurements	26
3.7.1. I-V Characterization of AR Coatings	27
CHAPTER 4. RESULTS AND DISCUSSION	30

4.1. SEM analysis of SiO ₂ doped thin films in small area	30
4.2. Optical characterization of small area	33
4.3. Solar spectrum I-V of small area	37
4.4. Photocatalytic Activity (MB) of small area	41
4.5. SEM analysis of SiO ₂ doped thin films in large area	44
4.6. Optical characterization of large area	45
4.7. Solar spectrum I-V of large area	49
4.8. Photocatalytic Activity (MB) of large area	51
4.9. Durability test	53
CHAPTER 5. CONCLUSION	55
REFERENCES.....	57

LIST OF FIGURES

Figure	Page
Figure 1.1. The spectrum of AM1.5 regarding the AM0 spectrum and the 6000k radiation distribution.....	2
Figure 1.2. The scheme of the band structure of the p-n junction.....	4
Figure 2.1. Spreading of light rays via a) on a substrate of single-layer thin-film b) on a substrate of the multilayer thin film.....	7
Figure 2.2. Spreading light rays onto the substrate through a single-layer film ($n_S > n$)..	9
Figure 2.3. Reflection of wavelength for two-layer ARC.....	10
Figure 2.4. Simulated characteristics of a multilayer coating for thin film a-Si photovoltaic.....	11
Figure 2.5. The scheme deposition techniques of AR thin films.....	12
Figure 2.6. The stages of the dip-coating process.....	14
Figure 2.7. Application of spray-coating technique via Computer controlled spray coating technique	15
Figure 3.1. The schematic of preparation solution in magnetic stirring device	16
Figure 3.2. The next step of preparation solution in magnetic stirring device	17
Figure 3.3. Schematic representation of Computer Numerical Control system	18
Figure 3.4. Images of coated and uncoated SiO ₂ -doped thin films	18
Figure 3.5. The process of dip-coating in small area	19
Figure 3.6. The process of spray-coating in large area using CNC system	20
Figure 3.7. Research room of SEM.....	21
Figure 3.8. The chemical representation of Methylene Blue (MB)	22
Figure 3.9. The absorption graph of methylene blue in individual wavelengths stimulation	22
Figure 3.10. The photocatalytic degradation of MB using a) discovered by GC/MC b) discovered by LC/MS	23
Figure 3.11. Representation of photocatalytic experiment with (MB) solution	24
Figure 3.12. Representation of adhesion test of AR coatings	26
Figure 3.13. The determination of distribution diffuse, direct, global solar radiation.....	27
Figure 3.14. A typical I-V curve and power curve characteristics of a solar cell	29
Figure 4.1. (a, b, c, d) SEM analysis of SiO ₂ coated thin films with different pulling speed.....	32

Figure	Page
Figure 4.2. (a, b, c,) SEM analysis of SiO ₂ coated thin films at different temperature....	33
Figure 4.3. UV-spectrophotometer transmission analysis with different pulling speed.	34
Figure 4.4. UV-spectrophotometer reflectance analysis with different pulling speed...	35
Figure 4.5(a). UV-spectrophotometer (%T) analysis with different keeping time in. solution	35
Figure 4.5(b). UV-spectrophotometer (%R) analysis with different keeping time.....	36
Figure 4.6(a). UV-spectrophotometer (%T) analysis with different temperature	36
Figure 4.6(b). UV-spectrophotometer (%R) analysis with different temperature.....	37
Figure 4.7. Scheme of a simple solar simulator	38
Figure 4.8. The solar cell simulator analysis of uncoated glass.....	38
Figure 4.9. The solar simulator analysis in small are for coated glasses.....	39
Figure 4.10. The solar simulator analysis of coated glasses in small area	40
Figure 4.11. The efficiency of coated glasses in small area	40
Figure 4.12. Degradation of Methylene Blue solution with bare glass	42
Figure 4.13. Photocatalytic degradation of (MB) solution with SiO ₂ coated glass	43
Figure 4.14. Degradation of Methylene Blue solution with SiO ₂ coated glass	43
Figure 4.15. SEM analysis of SiO ₂ coated thin films at 600°C for large area	45
Figure 4.16. Measuring %R analysis via UV-spectrophotometer with spray-coating ...	46
Figure 4.17(a). UV-spectrophotometer %R analysis via spray-coating method	46
Figure 4.17(b). Measuring %T via UV-spectrophotometer 600°C with spray-coating ..	47
Figure 4.18(a). UV-spectrophotometer %R analysis in 600°C via spray-coating	47
Figure 4.18(b). UV-spectrophotometer %T analysis in 600°C via spray-coating	48
Figure 4.19. The solar simulator analysis in large are for coated glasses	49
Figure 4.20. The solar simulator analysis of coated glasses in large area	49
Figure 4.21. The efficiency of coated glasses in large area	50
Figure 4.22. Photocatalytic degradation of (MB) with coated glass heated at 550°C....	51
Figure 4.23. Degradation of MB solution with SiO ₂ coated glass at 550°C	52
Figure 4.24. Degradation of MB solution with SiO ₂ coated glass at 550°C	52
Figure 4.25. Images of uncut glass a) under microscope and b) outside microscope	53
Figure 4.26. Images of cut substrate coated glass after removing scotch	54

LIST OF TABLES

Table	Page
Table 4.1. The results of solar simulator analysis for coated and uncoated glasses in small area.....	41
Table 4.2. The parameters of Z(height), P(pressure) and Y(interval)	48
Table 4.3. The results of solar simulator analysis for coated and uncoated glasses in large area	50

CHAPTER 1

INTRODUCTION

1.1. The Energy Power of Sun

Every hour the sun radiates an enormous amount of energy which provides people with sustainable, clean and renewable energy. Its beams hold the planet warm and make life feasible in a small globe. Each day it sends out huge energy that humans consume in a year (Augenbraun et al. 2010). The energy sun comes from itself which consists of atoms helium and hydrogen in a plasma condition, called process nuclear fusion. The main fusion process is integrating hydrogen isotopes to form a helium atom. The amount of energy that reaches the earth is approximately 173×10^3 (GW) while according to IEA the world's total energy demand in 2008 was around 13.7×10^3 (GW). Renewable, unlimited, and sustainable solar energy will be obtainable so far as the sun keeps on shining (Stocker et al 2014).

By directly and indirectly ways sunlight hits the surface of the earth. Direct irradiance is a total of sunlight without disruption obtained from the sun. But indirect solar irradiance is sent back (reflected) by other molecules in the atmosphere to get to the surface from all corners. On open days, direct radiation demonstrates 85-90% of solar energy. On misty days it substantially zeroes, while the indirect radiation represents about 100% of solar energy reaching the earth's surface.

About 7% of the total energy sun constituted of ultraviolet radiation, 46-47% (VR) visible radiation, and 47% of infrared radiation. Among them, visible and infrared radiations are used to generate energy by nature world and people. But ultraviolet radiation is filtered out by the ozone in the top atmosphere, which causes the destruction of many substances.

Solar energy had been used by people for centuries BC, in order to focus light from the sun and start a fire by using simple magnifiers. For the first time in France, solar collectors were used to manufacturing steam, while in the USA, solar water heaters became popular. People use solar energy today to employ in photovoltaic technology,

solar thermal energy, high-performance buildings and so on (Psomopoulos and Mardikis).

Having an idea of the solar spectrum and how it changes contingent on the environment and global situation will give us opportunities to expand effective technologies for using solar energy. The solar spectrum at the surface of the earth and in the upper atmosphere is different because of absorption by gases (dust, smog, ozone, and CO₂). Spectrum solar in the upper of the atmosphere and at the ground is compared in Figure 1.1.

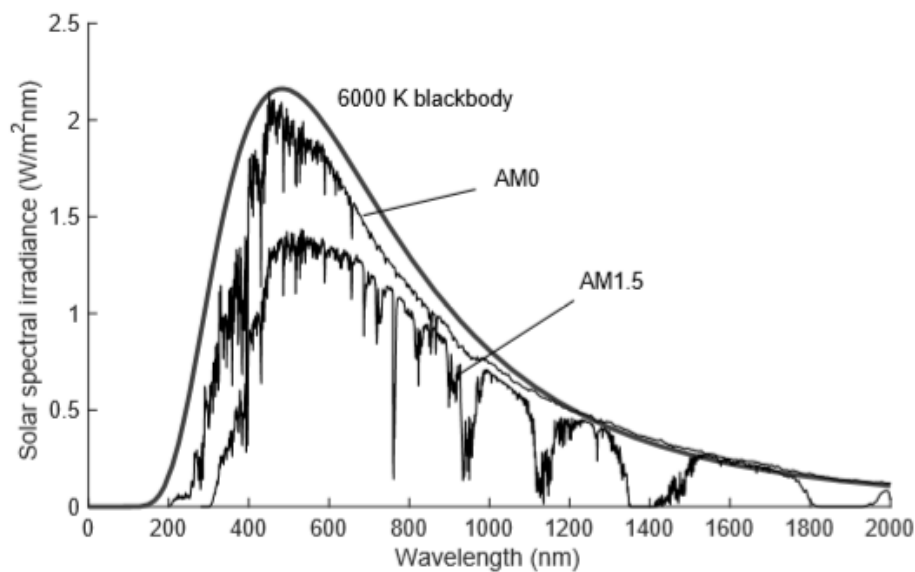


Figure 1.1. The spectrum of AM1.5 regarding the AM0 spectrum and the 6000k radiation distribution (Source: Riordan and Hulstron 1990).

The further radiation of the sun passes through the atmosphere, the fading it becomes. These changes can be observed over the course of months or on separate days, since the longest path occurs in the evening, as the sun approaches the horizon (Source: Riordan and Hulstron 1990). The air mass that describes the path length is the ratio of the mass of the atmosphere that the radiation travels from the current position of the sun over the sky toward the mass when the sun is in its zenith (Source: Piebalgs and Potocnik 2009).

1.2. Photovoltaic technology

Photovoltaic technology is the area of research connected to the systems which generate direct current electrical power in (W) or (kW) by illuminating photons from

semiconductors (Source: Piebalgs et al. 2009). Photons are using to thrill electrons into a thrilling condition by photovoltaic (PV) effect, therefore electrons are free and easily can move (Source: Luque and Antonio 2011).

Today, the use of solar panels to generate electricity has become popular in all regions of the country. New methods and technologies have been applied to create high-performance panels of lower cost. The basis of photovoltaic technology is solar cells. Semiconductor materials, like silicon, are used for manufacturing solar cells.

Any solar cell has p-n junction. Comprehension and modeling are very simplistic by applying p-n junction idea. For example, silicon has four valence electrons, and during the fabrication of a photovoltaic solar cell is being processed to grow its conductivity. The impurity cells, which present phosphorus atoms with five valence electrons n-side (negative charge), give low bound valence electrons to Si material. On the other hand, three valence atoms of boron p-side (positive charge) build greater proximity to draw electrons than silicon. When these materials get in touch with each other, electrons diffuse from the (n-type) into (p-type) and holes from (p-type) to the (n-type). Electrons integrate with holes on the (p-type) side when they diffuse through the p-n junction. But carrier diffusion does not happen infinitely, as the unbalance of charge directly on both sides of the junction occurs in an electromagnetic field. The created electrical field creates a diode that supports current to flow on one side. In both sides of the solar cell (n-type) and (p-type) Ohmic semiconductor contacts are performed, and the electrodes are available to be connected to the outer load. Energy is transferred to the charge carriers when it produced by falling photons of light on the cell. Photo-generated charge carriers (holes) separate by the electrical field in the junction from their negative equivalent (electrons). Thus, after closing the circuit on the outer load, the electric current is removed (Source: Piebalgs and Potocnik 2009).

Hetero and homo-junction are the main types of p-n junction. In homo-junction when (n-type) and (p-type) semiconductors are doped with the opposite charge but keep the same one material. The p-n junction is considered a hetero-junction when the materials are completely different. The scheme of the band structure of the p-n junction is displayed below in the Figure 1.2.

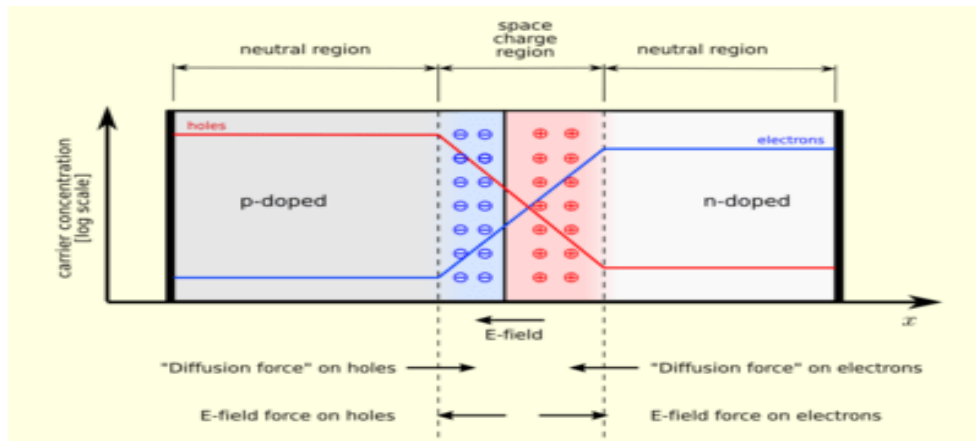


Figure 1.2. The scheme of the band structure of the p-n junction.

Different types of solar panels are produced worldwide. But 90% of them composed of wafer-based silicon. One of the leading areas in solar energy is the photo-conversion of solar radiation energy. The features of the silicon method of generating electrical energy are studied using solar cells to convert solar energy into electrical energy with photoluminescence of solar radiation, with radial p-n junctions in vertical microstructures.

Wafer-silicon, they are more widespread than the thin-film types of solar cells. The thickness of wafer-silicon solar cells is about 200 μm . Their popularity is due to several factors: the prevalence of silicon in the earth's crust by a large number of manufacturers, high efficiency and simpler manufacturing technology. High-purity silicon is used to produce single-crystal solar panels. The technology for the production of single-crystal panels is quite expensive, but it justifies its cost with high-efficiency modules (the highest value ranges from 18-22%). Poly-crystalline, they are made by slow cooling of the alloy, the basis of which is silicon. Poly-crystal is made using less pure and cheaper silicon. This technology, unlike monocrystalline, requires significantly lower energy consumption, so the cost of this type of solar panels is slightly lower. However, due to the granularity of the boundaries of their efficiency is slightly lower. Amorphous-silicon panels are made using not crystals, but very thin layers of silicon sprayed onto plastic. These batteries have the lowest efficiency (about 6%), but despite this, they are very popular due to their high optical absorption, effective performance at low brightness of sunlight and ultra-thin photocells (Source: Luque and Antonio 2011).

Thin-film solar panels are one more main family of thin-film solar cells with approximately 1-2 μm thickness. Because of this function, they demand less active semiconductor materials. Thin-film solar panels, these photocells are characterized by

lower performance and price. Cadmium telluride panels are manufactured using cadmium telluride. Previously, this technology was used only in astronautics, but now such panels are available for any home. And although the efficiency of such photo panels was not high, in recent models it is approximately 18% (Source: Guo et al. 2017). Polymeric, they have a small efficiency (only 6%), but because of their low cost, they are popular and are considered the most affordable.

1.3. Purpose of the Thesis

Solar energy currently one of the promising directions for the development of environmental sources of electricity since sunlight is the main and most accessible source of energy on Earth for living organisms. In an effort to curb this energy, we can reduce the overall human impact on the environment. Improving the efficiency of the panels is one of those things that reduce the cost of production and also provide cheaper solar panels. Thus, it is required to improve the conversion rate of incident sunlight into electricity, to increase the efficiency of solar cells. Improving efficiency is one of the priority areas of research centers. Because increasing the efficiency of PV significantly reduces the payback time, it allows you to get more electricity per unit area (saving on renting or buying land, it is also an important factor in conditions of shortage of space: for roof solar power plants). High efficiency is very expensive, but today researchers using various methods to get more effective results. Therefore, solar energy needs commercial creation and new options, also available methods must be sought to increase the efficiency of solar energy.

In all photovoltaic technology, the light loss into the cell approximately $\sim 4.22\%$ when it is air-glass at it. Antireflective coatings (ARC) is one of those ways to increase the efficiency of photovoltaic technologies. Through (ARC), we can achieve a decrease in the amount of reflected light at a specified interface. In chapter 2, the types of Antireflective coatings, deposition techniques of single-layer and double-layer ARC for thin-films are fully reported with a focus on SiO_2 . In chapter 3, is described all standard tests after applying ARC to solar panels, which evaluate the long-dated persistence of solar panels.

CHAPTER 2

THEORETICAL BACKGROUND

2.1. Antireflective Coatings

Anti-reflective coatings are used in a wide range of applications where light passes through the optical surface and low loss or low reflection is desired. Comprehensive research in the field of minimizing biological and optical reflection after the years helped anti-reflective coatings (ARC) have developed into highly efficient reflective coatings in different optic types of equipment. How we have mentioned above, in all photovoltaic technology, the photon flux into the cell approximately reduces to ~ 4.22% by reflection. Antireflective coatings (ARC) is a way to increase the efficiency of photovoltaic technologies. Through (ARC), we can achieve a decrease in the amount of reflected light at a specified interface.

When the nature of reflection is known, the development of effective ARC is very simple. Typically, reflection happens at the interface among the two materials. The percentage of reflection depends on the polarity of the light, the magnitude of the dissimilarity between (RI) of the layers, and the incidence of light in the corner of the interface. By the equation shown below reflection can be characterized (Source: Fowles, at al. 1989).

Reflection is born in a medium in which light moves. The refractive index (n) which characterizes the medium, measures the speed of light compared to the speed of light in a vacuum. So, during the propagation of light, if there is a change in the refractive index (RI) the eyes can detect an optical disruption, and this is the Fresnel equation. According to equation Fresnel, the fraction of reflected falling light at the interface is determined by (R), and the remainder of the transmitted light by (T).

The vector method in mathematical form examines a thin film (RI = n) on a substrate of glass (RI = n_s) to determine the antireflective condition as said in Figure 2.1. and makes the next suppositions.

- At the interface, the reflected wave has one reflected and the same intensity.
- Scattering, absorption, and different optical interactions are insignificant.

As shown in Figure 2.1(a), there will be no reflection, if the reflected waves R1 and R2 are suffered to destructive interference, destroying each other and two main criteria for Anti-Reflection is followed.

- (π) radians are the reflected waves out of phase and $[\delta \text{ is } n\pi/2]$.
- (d) is the diameter of the film and is an odd multiple of $(\lambda/4)$, where (λ) is the wavelength of falling light.

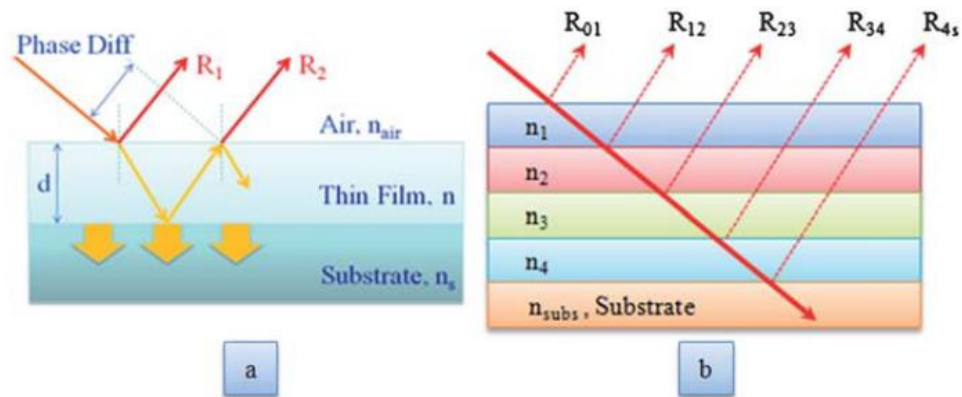


Figure 2.1. Spreading of light rays via a) on a substrate of single-layer thin-film b) on substrate of the multilayer thin-film (Source: Raut, et al. 2011).

The equation phase difference equal to $\delta = 2\pi nd \cos \theta / \lambda$. Replace the value of (δ) and (d) the $Q=0$, and it is a relative incidence. The following formula below is for reflectance at relative incidence.

$$r = \left[\frac{n_{air}n_s - n^2}{n_{air}n_s + n^2} \right]^2 \quad (1)$$

Where n_s is the (RI) of the substrate, n_{air} is (RI) of the air and $n =$ (RI) of the film.

The last analyses were based on a single layer on a substrate, and for multilayer ARC the basics remain the same. But the only dissimilarity is the mathematical model, which depends on vector analysis singular rays. The reflected light between neighbor layers (i) and (j) from the user interface (i, j) is defined as:

$$R_{ij} = |R_{ij}| \exp[-2(\delta_i + \delta_j)] \quad (2)$$

As $|R_{mn}| = [(n_i - n_j)/(n_i + n_j)]$ is equal, so by $\delta_i = 2\pi n_i \cos \theta_i d_i / \lambda$ the phase thickness of layers is determined. Where, Q_i is an angle of reflective, d_i the thickness of layers, λ the wavelength of incident light. From the figure 3(b) it is quite obvious that reflection vectors form from the (i, j) interfaces. The obtained reflection vector is explained by:

$$R_{sum} = R_{01} + R_{12} + R_{23} + R_{34} + R_{4s} \quad (3)$$

Where, $R_{01} = |R_{01}|$

$$R_{12} = |R_{12}| \exp[-2(\delta_1)] \quad (4)$$

$$R_{23} = |R_{23}| \exp[-2(\delta_1 + \delta_2)] \quad (5)$$

$$R_{34} = |R_{34}| \exp[-2(\delta_1 + \delta_2 + \delta_3)] \quad (6)$$

$$R_{4s} = |R_{4s}| \exp[-2(\delta_1 + \delta_2 + \delta_3 + \delta_4)] \quad (7)$$

By modifying the (RI) and thickness film or by decreasing the R_{sum} in each layer, an anti-reflection condition will be obtained.

2.1.2. The Single Layer ARC

Single-layer is the simplest form of AR-coatings that are used for a very wide spectral range (450–1100 nm), to reduce the reflection ability to (2.6–2.5%). The choice of material is a complex and main task because the use of a single-layer ARC is little by the presence of suitable material since RI for glass is about 1.49-1.50 and RI for thin-film coating should be 1.21-1.22. But unfortunately, materials with low (RI <1.22) are not very, but (MgF₂) the most used in single-layer ARC. With (magnesium fluoride n=1.37) it is possible to reduce the reflection surface from 4.3 % (no coated glass) to roughly 1.6% (Source: Raut, et al. 2011).

Subject to that the substrate index is greater than the film index when the incident medium is air, then a phase change of 180 degrees occurs and this means that the

reflective index at the interface will be negative. The phase diameter of the layer or the quarter-wave optic diameter is (90°) when the vectors are opposite to each other. If the vectors are the same length, there will be a complete suppression at zero reflection (Source: Macleod, et al. 1986).



Figure 2.2. Spreading light rays onto the substrate through a single-layer film ($n_s > n$). (Source: Raut, et al. 2011).

2.1.3. Double Layer ARC

Double-layer ARC, consisting of two antireflection layers, the layers on the outside has a lower refractive index. It has a higher performance than a single layer coating and reduces reflectivity more than a single-layer coating (Kavakli, et al. 2002).

Applying double-layer ARCs, which each layer has a quarter wavelength thickness, able to increase the efficiency of ARC if $n_1 > n_s$ and $n_2 < n_s$ onto the SLG ($n_s=1.5$) substrate. As seen in the figure, this is the best option that leads to an improvement in the design of the AR effect. The reflection coefficient (Rf) of two-layer coatings in the wavelength region of ~ 550 nm significantly reduces and moves to zero. The two-layer ARC has a V-formed spectrum and because of the V-formed of their profile, they are called V-coated frequently (Chattopadhyay, et al. 2010).

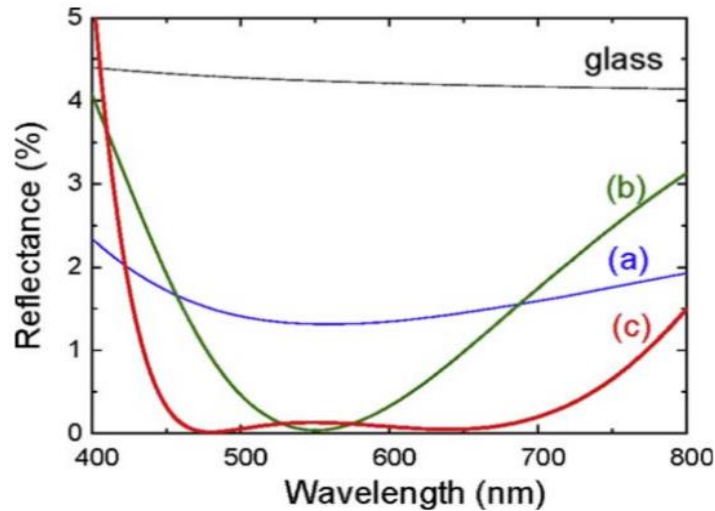


Figure 2.3. Reflection of wavelength for ARC (Source: Raut, et al. 2011).

2.1.4. The Multilayer ARC

A multilayer antireflection coating is a sequence of at least three alternating layers of materials with different refractive indices. The main advantage of multilayer illumination as applied to photographic and observational optics is the insignificant dependence of reflectance on wavelength within the visible spectrum (Source: Macleod, et al. 1986).

An alternative to multilayer antireflection coatings are layers with a continuously changing refractive index. The use of such coatings allows one to achieve low reflectance values in a wide spectral range. However, this method also has its drawbacks, among which there is a mismatch between the temperature expansion coefficients of the resulting layers and adhesion (Source: Macleod and Clark 2012).

The structure of Multilayer ARCs, using optical forming software, comparable to CdTe design was designed. Using a transfer matrix method based on destructive interference, coatings to minimize reflection were optimized. Using a transfer matrix method based on destructive interference, coatings for minimizing reflection were optimized. Coatings used thin films such as CdTe, CIGS and a-Si are optimized in the wavelength ranges to maximize production (Source: Kern, et al. 1970).

Comparing the bandgap of CdTe and a-Si solar cell ($\sim 1.7\text{eV}$), a-Si is higher, so the wavelength range is contracted to diapason 340nm to 740nm. The table down shows the form of four-layer ARC intended for application on (a-Si). This value for the coating structure decreases the Multilayer ARC from 4.2% for non-coated glass in the corresponding wavelength-range (360nm-710nm) until 0.6%. Thus, the Multilayer ARC

provides a-Si solar cells produce a high current density of ($J_{SC}=24.48\text{mA/cm}^2$). Compare to non-coated glass 3.7% is higher (Source: Kern, et al. 1970).

A simulated reflective spectrum with coated and non-coated multilayer antireflection shown in the below Figure 2.4. The blue line the front side is coated, the black line the back and front side coated, and the last line is red which back and the front side of the non-coated glass.

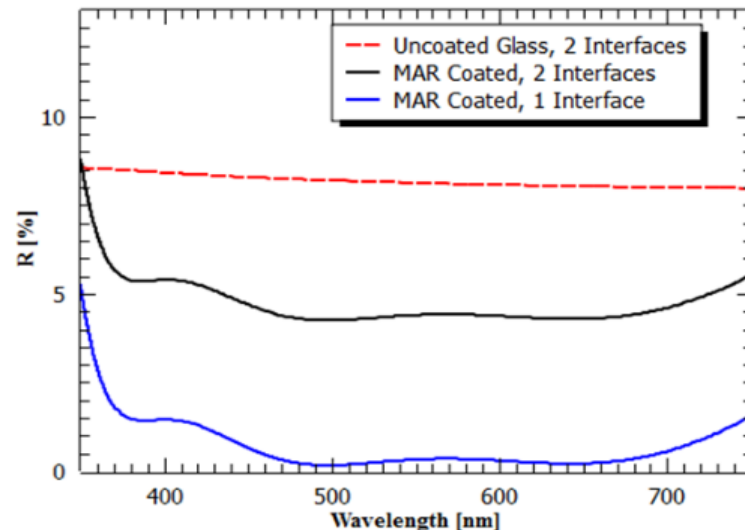


Figure 2.4. Simulated characteristics of a multilayer coating for thin-film a-Si photovoltaic (Source: Womack, et al. 2017).

2.2. Deposition Techniques of AR for Thin Films

In the deposition techniques section, the manufacturing methods that are used for AR structures will be considered. As a rule, manufacturing methods selected for this target can be grouped onto a bottom-up manner. Films or nanomaterials growth paths, as sol-gel processing, dip-coating, spray-coating, physical and chemical vapor deposition are used in the bottom-up method. The scheme deposition techniques of AR thin films are shown in Figure 2.5 (Source: Chattopadhyay, et al. 2010).

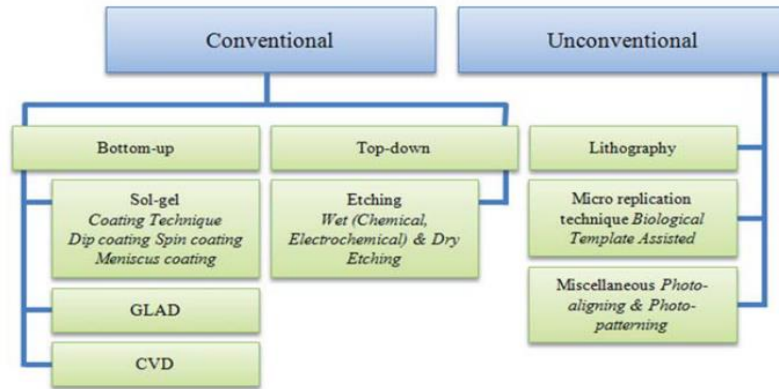


Figure 2.5. The scheme deposition techniques of AR thin films (Source: Raut, et al. 2011).

As we mentioned above, film deposition methods are divided into physical (Physical Vapor Deposition) and chemical (Chemical Deposition). Physical methods are based on the transport of film material in atomic form from a solid-phase source or target to a substrate, followed by condensation and coating formation (Source: Fouad and Ismail, 2006). The chemical methods are based on the deposition of gaseous or liquid precursors and the formation of a film as a result of chemical transformations of the precursors on the surface of the substrate or in the immediate vicinity of it.

2.2.1. Sol-gel Process

Sol-gel is one of the most common technologies that is used in the preparation of oxide nanoparticles, ceramics, and also thin films. Rather method which from small molecules produces solid materials. The main advantage of the sol-gel method is the high degree of homogenization of the starting components, which is achieved by dissolving the salts and oxides of the starting materials in the solution. As a result, it becomes possible to significantly reduce the temperature of the synthesis of materials (Source: Pagliaro, et al. 2009). A significant advantage of the method is the ability to easily control the composition of the material by changing the concentrations of the starting components in the solution. The advantage of technology is the ability to get thicker films than from true solutions (Source: Brinker, et al. 1990). In anti-reflective coating (SiO_2) most commonly used, that accumulates with the sol-gel technique. For application AR coatings the materials with a low refractive index more advantaged such as silicon dioxide or magnesium fluoride, but silicon dioxide (SiO_2) holds more mechanical

durability and air-hole portion inside the film is increased than mentioned materials. Another aspect is to take control over the scale of the microstructures into surfaces of sol-gel, as surface capacity, empty radius, and area (Source: Brinker and Scherer, 1990).

Because of the wide advantages, sol-gel solutions own various characteristics, such as hydrophobicity and antistatic AR coatings that have beneficial properties (Source: Oishi, et al. 1999). Reflectance can be decreased due to sol-gel methods at the air-glass interfaces up to 0.7% by giving an appropriately designed coating. Thus, coatings that have adequate adhesiveness and mechanical durability characteristics have been prepared on plastics and glasses (Source: Chen, et al. 2001).

2.2.2. Dip-Coating method

The dip-coating method is used to create thin films and coatings. It is quite simple, which makes it easy to automate. The dipping method is a process in which a substrate is immersed in a liquid and then removed under controlled environmental conditions, which finally leads to coating. The thickness of the coating is determined by the rate of rising of the substrate, the viscosity of the liquid and the content of solid components. If the substrate lifting speed is selected considering that the state of the system will be in the Newtonian regime, then the film thickness can be calculated using the (Source: Landau-Levich) equation below (Source: Strawbridge and James. 1986).

$$h = 0.94 \cdot \frac{(\eta \cdot \nu)^{2/3}}{\gamma_{LV}^{1/6} \cdot (\rho \cdot g)^{1/2}} \quad (8)$$

Where, (h) is the thickness of the coating, (η) is the viscosity, (γ_{LV}) is the surface tension of the liquid-vapor, (ρ) is the density, and (g) is the specific gravity (Source: Brinker and Scherer. 1990).

The dip-coating method can be divided into three main stages: the substrate is dipped into the solution at a constant speed, keeping the substrate in solution in a stationary state and the substrate is removed at a constant speed (Source: Brinker, et al. 1990). The faster the substrate is removed from the solution, the thicker the layer of material on the substrate will be. An interesting effect arises in the dip-coating method: by choosing the suitable viscosity, the coating thickness can change with high precision

from 20 nm to 50 μm while keeping high optical quality. A diagram of the dip-coating method is shown in the Figure 2.6 (Source: Lide, et al. 1998).

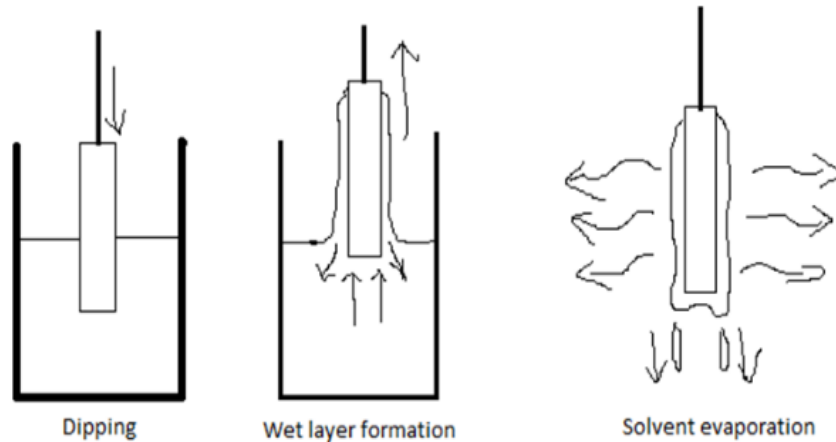


Figure 2.6. The stages of the dip-coating process: dipping of the substrate in a solution, the formation of a wet layer by removing the substrate and converting the layer into a gel by evaporation of the solvent (Source: Yao and He. 2014).

2.2.3. Spray Coating Method

Spray-coating technique is used to produce spray on the surface of glasses (thin films) via the CNC-machine system. The main parts of the machine consist of:

Computer-Aided Design (CAD), it is called the designer part that generates Part-Program. This part defines the mechanism step, usually written on (G-Code). Machine-Controller another part of machine the output files of (CAD) is transferred by network links or USB drive. It reads and deciphers Part-Program in order to take control of a tool. (Mach-3) makes the functions of Machine-Controller which working on PC, transfers a signal to the driver. Drivers also one of the main parts of the CNC system machine, this part is suited timed and enough powerful. The main mission of this part is to get a signal from Machine-Control, strengthen it and run the motor driving the mechanism. Screws, belts racks are the tools that the machine is removed by them.

Nitrogen (N_2) tube with (...) capacity. Gas regulator belongs to (N_2) gas. This regulator will determine the capacity of the tube inside and how much gas will be released outside. Z-nozzle with (0.22 bar), S-nozzle with (0.6-.07 bar) and W-nozzle with (0.5-1 bar) pressure bonded to a container of a solution with a 50mL capacity. The compressor is the main part to provide spray droplet carrier airflow. Changing the pressure and the

parameters nozzles, it is possible to get different results for the spray-coating method on the surface of glasses.



Figure 2.7. Application of spray-coating technique via Computer controlled spray coating technique.

CHAPTER 3

EXPERIMENTAL PROCEDURE

3.1. Preparation of AR Solution

1.18 g of polyacrylic acid (PAA) with 22 mL (ammonia solution 25%) was mixed. After that kept on magnetic stirring for 5 min. This mixture was dissolved in 440 mL of ethanol and again kept under spirited magnetic stirring. The first time it was added 200 mL of ethanol and mixed for 30 min under magnetic stirring. After 30 min again was added 50-100 mL of ethanol, but this time it was kept for one hour under magnetic stirring with the high speed. Thus, in total 440 mL ethanol was added.

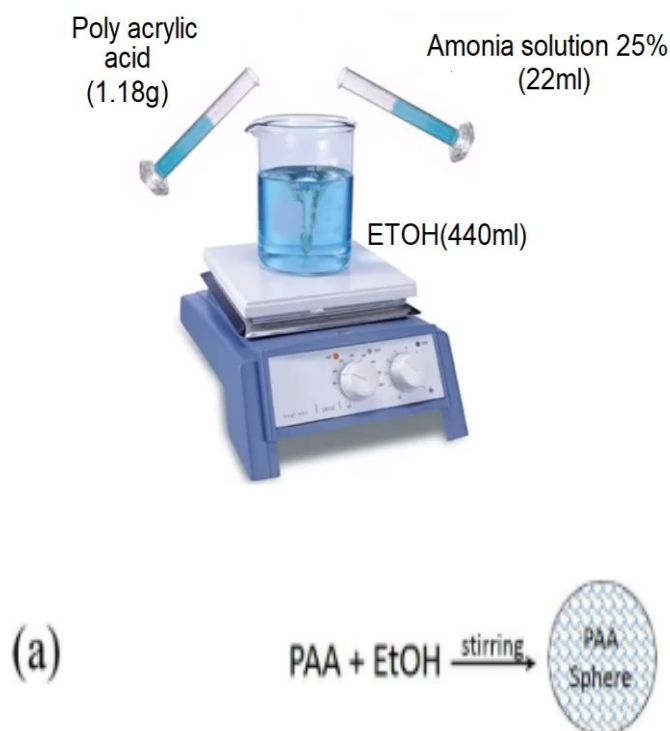


Figure 3.1. The schematic of preparation solution in magnetic stirring device.

At stable temperature of room under magnetic stirring, 5 mL of Tetraethyl-Orthosilicate (TEOS) was injected into mixture, 1mL (TEOS) in 1 hour. Thus, it was added 5 mL in total in 5 hours with keeping beaker on magnetic stirring.

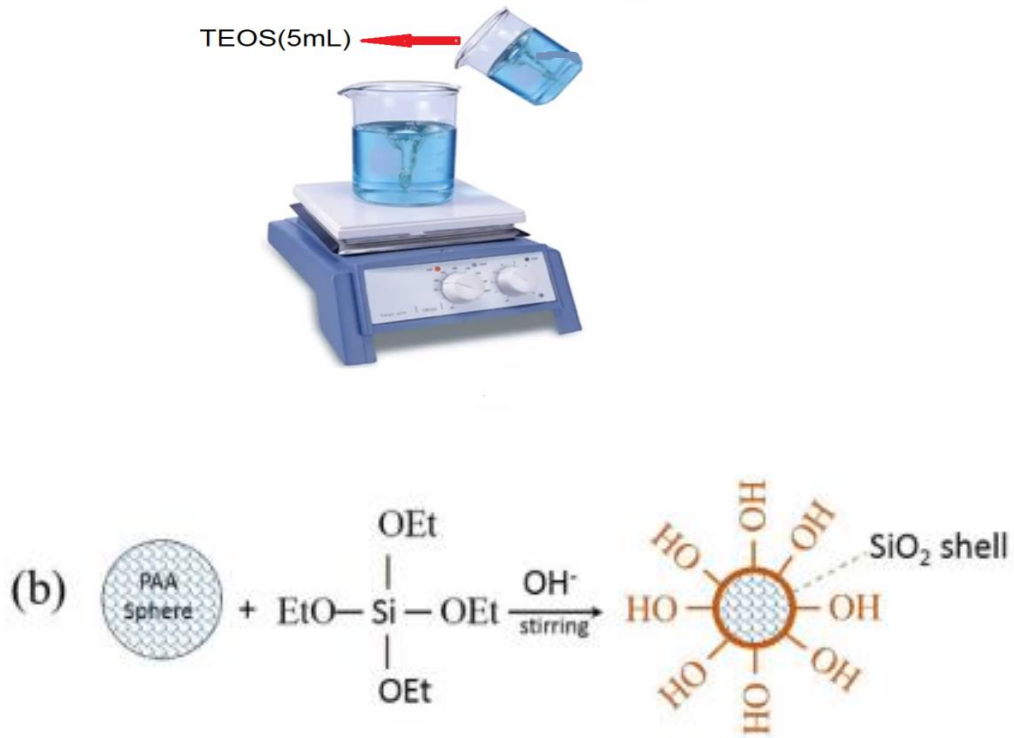


Figure 3.2. The next step of preparation solution in magnetic stirring device.

After all of this, the solution was hold for 12 hours more with constant temperature and speed under stirring at room. After 12 hours, 50 nm-60 nm (SiO₂) nanoparticles were created. By refluxing the solution for 8 hours at 90°C the ammonia was removed (Source: Guo, et al. 2017).

3.2. Fabrication of AR Thin Film

First of all, soda-lime glass was washed in detergent, then ultrasonic cleaning in deionized water for 6-8 min. Then the glass slides were cleaned by flushing of ethanol and dried with an unsalted napkin. Of course, the small area and large are AR coatings were applied by CNC system. The spindle drives are the main part in immersion and removing samples in dip-coating method and for spraying solution in spray-coating method is controlled by part program controller. After writing (G-code) the processes are

started. The cleaned glasses were dipped into the solution and were removed back again. The samples after the dip-coating and spray-coating methods were kept at room temperature for 10-15 min to dry.

In the end, the organic particles on the surface glasses and PAA templet were removed by thermal treatment process in the air (via putting samples in the oven at different temperatures 525°C -550°C -600°C for 1 hour and 24 hours) to form the closed-surface AR thin films.

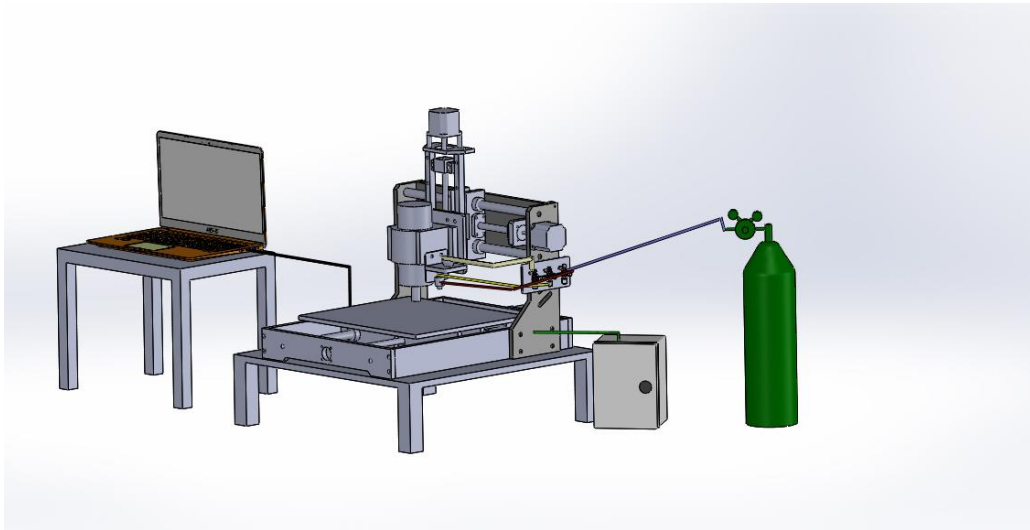


Figure 3.3. Schematic representation of Computer Numerical Control system.

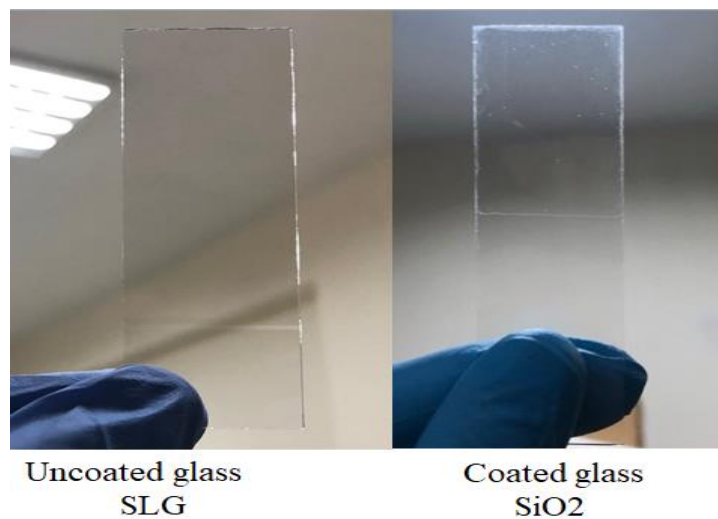


Figure 3.4. Images of coated and uncoated SiO_2 -doped thin films.

3.2.1. Small Area AR Coatings by Dip Coating Method

Small area AR coatings by the dip-coating method were applied by the CNC system. First of all, the sample was fixated in spindle drives. The spindle drives controlled by part program controller. After writing G-code the process is started.

The samples were dipped into the solution with 2.5mm/sec and were kept for 30 sec on it and with 2 mm/sec were removed from solution. After removing they were dried at room temperature and were heated at 550°C -600°C in the oven for 1 hour and 24 hours.

Testing of solution prepared in small sizes (3 cm to 3 cm) on sample glasses. The analysis was tried in different conditions and the received results are shown down in the next chapter.

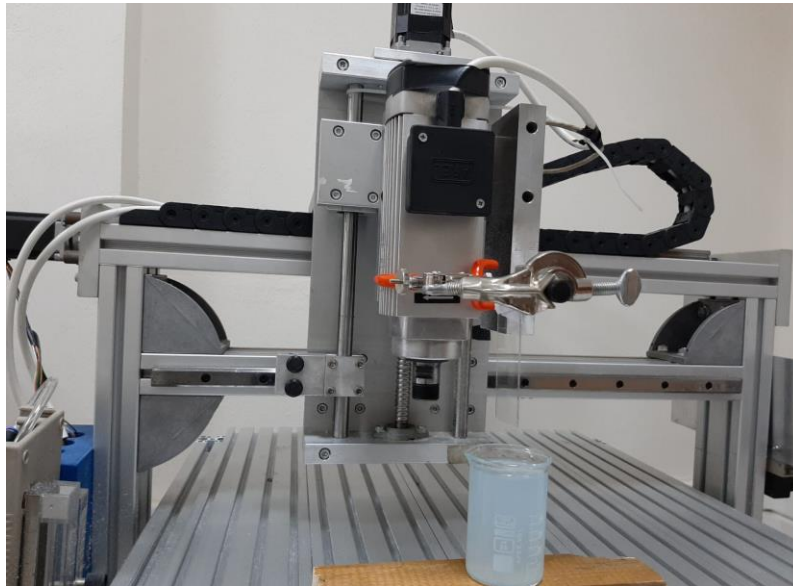


Figure 3.5. The process of dip-coating in small area.

3.2.2. Large Area AR Coatings by Spraying-Coating Method

The testing of the solution was prepared in large sizes (50 cm to 50 cm) on sample glasses with a spray-coating method via a CNC system. Before starting the process, the container (50 mL) was filled with a solution and cleaned sample glass was placed under spindle drives. The needed option is entered in the (G-code) part program with the parameters (x, y, z). The next step was an opened gas regulator that belongs to (N₂) gas. The regulator was provided the amount of gas released outside. Z, S, and W-nozzle

bonded to a container of a solution. After finishing the preparation, the process was started and because of having a large area had taken a long time to finished. The coated sample glass was dried at room temperature for a time and again was kept in the oven at 525°C for 1 hour. After cooling, the characterization of samples was taken and compared in terms of performance and durability.

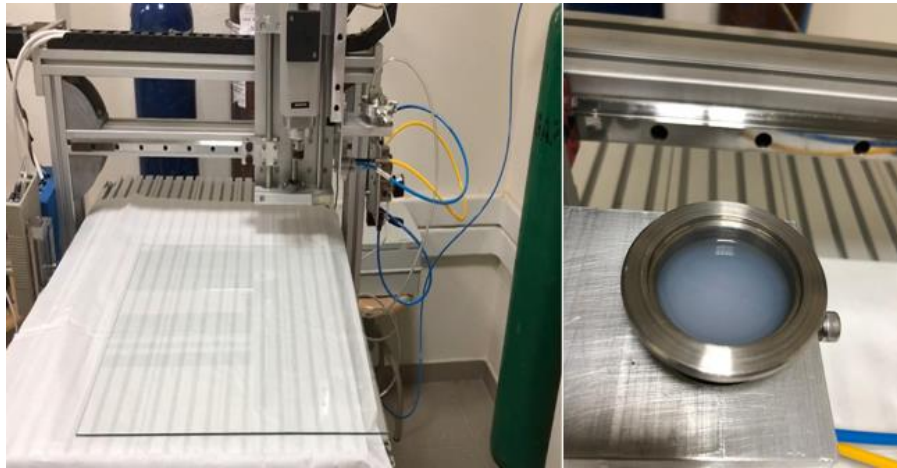


Figure 3.6. The process of spray-coating in large area using CNC system.

3.3. Optical Characterization of AR Surfaces

The (SiO₂) nanoparticles surface was obtained, and the characterization of the films was observed. The transmission (%T) and reflection (%R) of coated and uncoated films after fabrication sol-gel methods were measured using UV-vis-NIR spectroscopy. The EDX analysis and surface morphology of films, using SEM (Scanning Electron Microscopy) were conducted. Before SEM characterization for the surface morphology some of the samples were coated with gold film.

3.3.1. SEM Analysis

The scanning electron microscopy (SEM) analyses were realized in a FEI QUANTA 250FEG device. The morphology and microstructure characterization of thin films were observed.



Figure 3.7. Research room of SEM.

3.4. UV Spectrophotometer Measurements

The spectrophotometer measurements were realized in UV-vis-NIR Perkin Elmer Lambda 950 in the wavelength range of 200-2600 nm which owns controllable spectral band-wideness. The transmission and reflection of coated and uncoated thin films were investigated in range of 200-2600 nm with a scanning step size of 4nm. Also, the optical absorption of thin films was determined in the wavelength range of 300-700 nm at room temperature.

3.5. Photocatalytic Degradation of Methylene Blue Dye Test

This study was devoted to the improvement of a low-cost and fast technique for the deletion of the color dye from water by using SiO₂ nanoscale semiconductors as photocatalysts. The kinetic photocatalytic degradation researches were performed on methylene blue solution with doped SiO₂ thin film which in the bottom of the beaker was illuminated by UV-light source. Various factors impacting the process was studied as dye concentration and catalyst concentration of a solution. Methylene blue has a C₁₆H₁₈N₃SCl formula and is a brightly colored cationic thiazine dye which explained in figure. The absorption variation was determined at different bands (663, 292 and 246 nm) as shown in Figure 3.8.

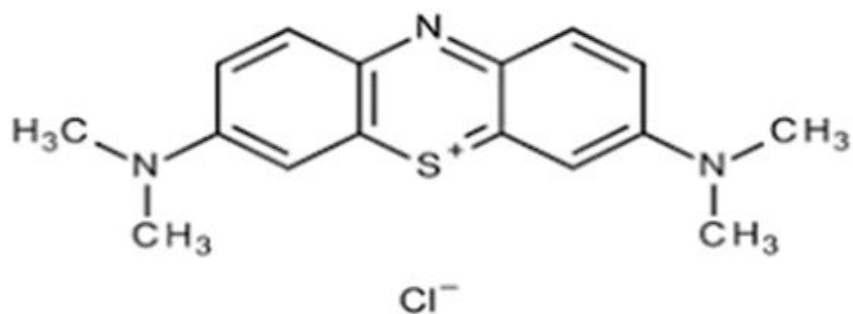


Figure 3.8. The chemical representation of Methylene Blue (MB).

In studies on photocatalytic degradation, all chemicals were of analytical quality and were used as they were. Methylene blue (MB) which at least 97% pure was ordered from Sigma-Aldrich and a solution of methylene blue obtained with de-ionized water (H_2O) and used as an organic admixture.

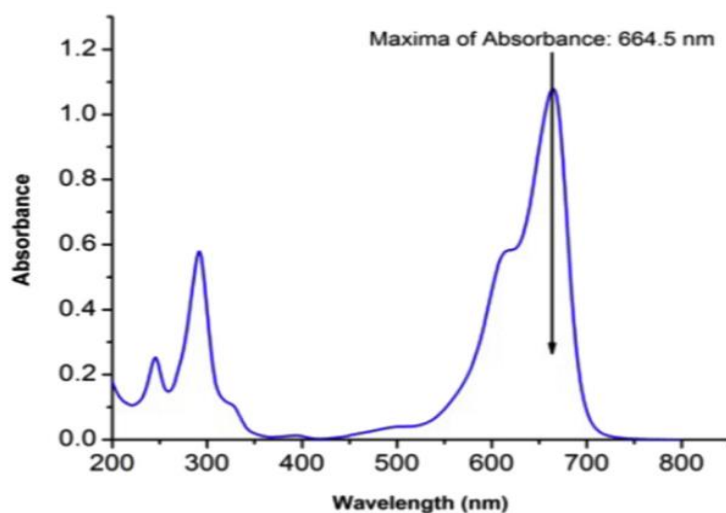


Figure 3.9. The absorption graph of methylene blue in individual wavelengths (Source: Zou and Gong 2016).

Via UV-vis spectrophotometer the absorption values of the obtained solutions methylene blue were appreciated. The calibration curve should be obtained at a wavelength of 664 nm that is the maximum value. The degradation pathway of methylene blue is in the figure 3.10.

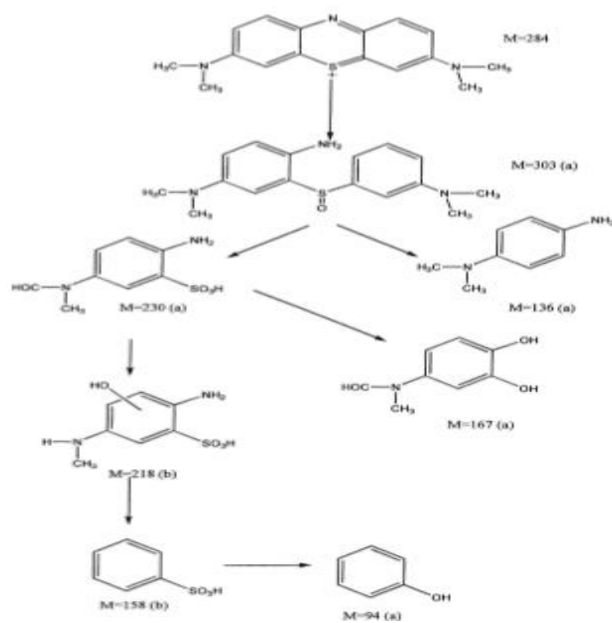


Figure 3.10. The photocatalytic degradation of MB using a) discovered by GC/MC b) discovered by LC/MS (Source: Houas, et al. 2001).

In preparation of MB solution, 20 mL and 1×10^{-5} M aqueous solution of methylene blue filled in an 80 mL beaker and SiO₂ coated glasses (3 cm x 3 cm) were placed into solution. About 2.5 mL of the prepared solutions were used for primary absorbance values. And for each coated glass UV-Vis spectrophotometer measurements were taken in (0, 1st, 2nd, 3rd, 4th, 5th and 24th hours respectively). Using absorbance values the concentrations would be calculated for each step of MB solutions by Beer-Lambert Law.

$$A = \epsilon \cdot b \cdot C \quad (9)$$

Where A is the absorbance, ϵ molar absorption coefficient, C is concentration and b are optical path length. The ϵ of the liquid is described by the path length and concentration by the light.

$$A = -\log\left(\frac{b}{b_0}\right) \quad (10)$$

Where A is the absorption value of MB at 664 nm, and for liquids absorption (A), the density of the falling and transmitted light is relatively b and b_0 . Thus, the concentration could be determined if the value of absorbance is measured.

$$\left(\frac{A_1}{A_0}\right) = \left(\frac{C_1}{C_0}\right) \quad (11)$$

Methylene blue (MB) solution (20 mL) with doped SiO₂ thin film (3 cm x 3 cm) in the bottom of the beaker was illuminated by UV source (Philips, TUV 16W GJ6 T5) 20 cm away. The solutions were illuminated with a 1-hour intervals under UV light then were taken for measurement of degradation MB absorbance by UV-vis spectrophotometer. After the measurement samples were settled into beakers again and the analysis was repeated.

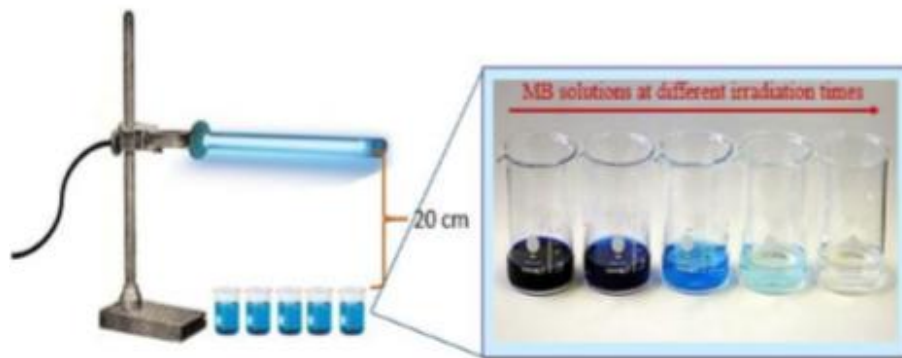


Figure 3.11. Representation of photocatalytic experiment with (MB) solution.

In some literature sources as (Source: Dean and Gomes, 2001) described a scheme in which the photocatalytic process occurs in the presence of organic pollutants and when a semiconductor catalyst is spread with an ultraviolet radiation source. The obtained nano-silica in this study performs function semiconductors and the next decomposition steps could be offered (Source: Kern, et al. 1970 and Chattopadhyay, et al. 2010).

e^- and h^+ production



e^- and h^+ capturing





In a formula, the SiOH explains the initially hydrated surface of SiO₂, e_{cb} represents a conduction-band electron and e_{tr} is captured conduction-band electron, h_{vb}⁺ valence-band hole, (Si^{IV}OH⁻) + surface-captured VB hole and (Si^{III}OH) surface-captured CB electron.

3.6. Adhesion Test of AR Coatings

Is it possible to appreciate adhesion considering the complexity of the test? The answer will be like yes and no as Mittal has commented in research. Currently, there is no test that could accurately determine the actual physical durability of adhesive bonds. But on the other hand, we can say that it is possible to get an indicator of relative adhesion productivity. One of the important factors for coatings is adhesion. Since high adhesion leads to more durability on thin-film photovoltaic modules. The adhesion test of AR coatings was determined using the tape-and-peel test and the tests were implemented on 2 mm thick SLG (Source: Mittal, et al. 1978).

Obviously, the tape and peel test are the most common test for understanding the adhesion of the AR coating. This test has been used in this area since the 1930. Taking a piece of adhesive tape and press it to the paint film, when removing the tape, the degree of removal and resistance of the film is followed which is the simplest version of the test (Source: Womack and Isbilir, 2019).

The test that was used is not very expensive. It is widespread and considered simple. After years of using the tape test, it will be comfortable to all, and as applied to substrates, it is cost-effective (Source: Wu, et al. 1982). Applied adhesive tape to a coated substrate glass and then removed from surface, the process is defined in fig. In the next chapter it is given more information about adhesive tape test. (Source. Wu, et al. 1982 and Nelson, et al. 2010).

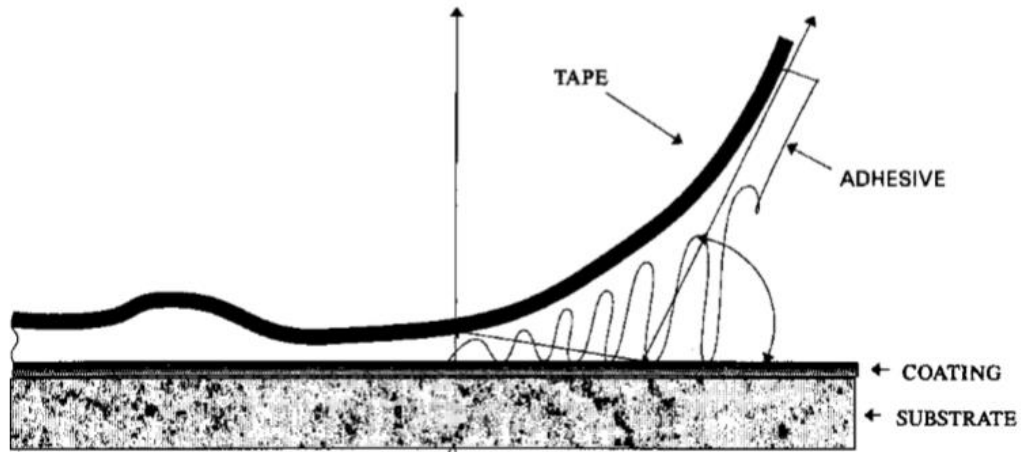


Figure 3.12. Representation of adhesion test of AR coatings (Source: Raheem, et al. 2019).

3.7. Solar Radiation Measurements

In this part the general term for electromagnetic radiation is solar radiation which radiated by sun. Extraterrestrial solar radiation or TSI is the total amount of solar radiation obtained at normal incidence in the upper part of the atmosphere at an average solar-earth interval. For a small amount, changing in TSI over time, a change in magnitude and variations directly or indirectly acts the atmospheric and biological processes on Earth. Almost to all models of solar radiation for estimating solar intensity radiation is used the solar constant, the value of which is defined as the intensity of solar radiation on the surface normal to the Sun's rays, directly outside the Earth's atmosphere at an average distance of the Earth from the Sun and is ($E_{sc} = 1367 \text{ W/m}^2$) (Source: Stackhouse, et al. 2011). Due to the fact that the Earth rotates around the Sun in an elliptical orbit, the extraterrestrial radiant flux from the Sun changes during the year, reaching a maximum in early January and a minimum in early July (Source: Lysko, et al. 2014). For the determining the solar radiation at the boundary of the Earth's atmosphere the given formula is followed.

$$E_0 = E_{SC} \left\{ 1 + 0,033 \cos \left[360^\circ \frac{(n-3)}{365} \right] \right\} \quad (16)$$

Where the n is the days of year (Source: Handbook, et al. 2009).

Solar radiation as passes through the Earth's atmosphere, it is redistributed. Therefore, according with its spreading, it is essential to look at the radiation of solar. The distribution of solar irradiance is explained in Figure 3.13, and there are three basic components: direct, diffused and the global solar radiation.

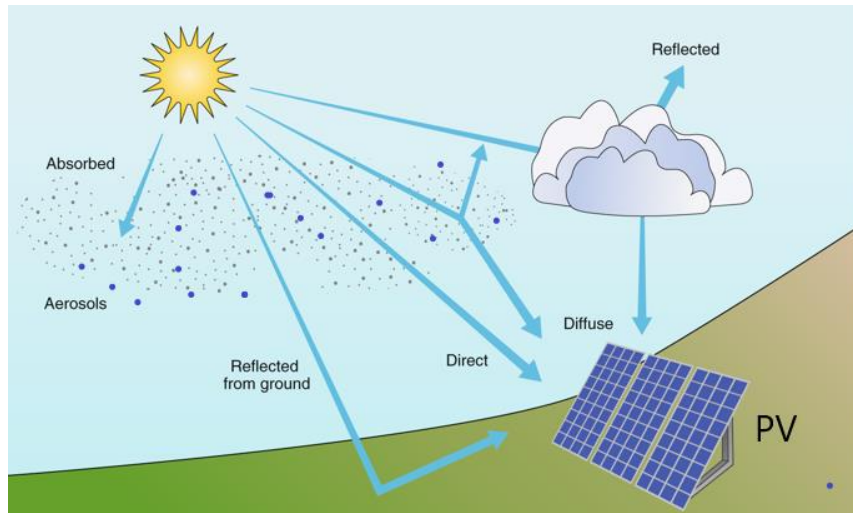


Figure 3.13. The determination of distribution diffuse, direct and global solar radiation (Source. Lysko, et al. 2014).

Diffuse radiation is received from the sun after reflection and scattering by the atmosphere and the earth. Sunlight obtained indirectly as a result of scattering due to clouds, fog, dust, or other obstructions in the atmosphere. The direct or beam radiation is called when the irradiance incoming to the Earth directly from solar circle. In practice, direct rays from the diffuse component differ in that the directed flow can be focused. The sum of diffuse and direct solar radiation is called total solar radiation which is termed global solar radiation (Source: Battles, et al. 1995 and Fainman, et al. 1992).

3.7.1. I-V Characterization of AR Coatings

The I-V Characteristics Curve of solar cell is a superposition of I-V-curve in the absence of darkness and when the light is available. Where the power can be extracted from diode, the I-V curve will be shifted by illumination. Giving a light to cells add to the normal darkness current in diode and we get the diode law as: (Source: Chen Fengxiang, et al. 2010).

$$I = I_0 \left[\exp \left(\frac{qV}{nkT} \right) - 1 \right] - I_L \quad (17)$$

Where, I_0 -is dark saturation current, q - charge, V -applied voltage, T -temperature and I_L - the light generated current.

From the I-V characterization some parameters are determined for solar cells. And these parameters are widely explained in figure below. I_{SC} is short-circuit current which current through solar cell when voltage is zero across the solar cell.

$$J_{SC} = qG(L_n + L_p) \quad (18)$$

Where L_n and L_p are (e^- and h^+) diffusion lengths, G is generation rate.

V_{OC} -open-circuit voltage which at zero current obtains the max. voltage from solar cell.

$$V_{OC} = \frac{nKT}{q} \ln \left(\frac{I_L}{I_0} + 1 \right) \quad (19)$$

The other parameter is (FF)-Fill Factor which in conjunction with (J_{SC}) and (V_{OC}) defines the (P_{MAX}) from a solar cell. The Fill Factor is determined as the ration (P_{MAX}) of solar cell to the (J_{SC}) and (V_{OC}).

$$FF = \frac{V_m \times I_m}{V_{oc} \times I_{sc}} = \frac{P_{max.}}{V_{oc} \times I_{sc}} \quad (20)$$

The most used parameter is efficiency, which compare the productivity of solar cells between each other. This parameter is determined as the ratio of extracted energy from solar cells to entrance energy the sun is send. And the efficiency of PV systems as a percent is explained: (Source. Emery and Osterwald, 1986).

$$\eta = \frac{P_{max.}}{P_{inc.}} = \frac{V_{oc} \times I_{sc} \times FF}{P_{inc}} \quad (21)$$

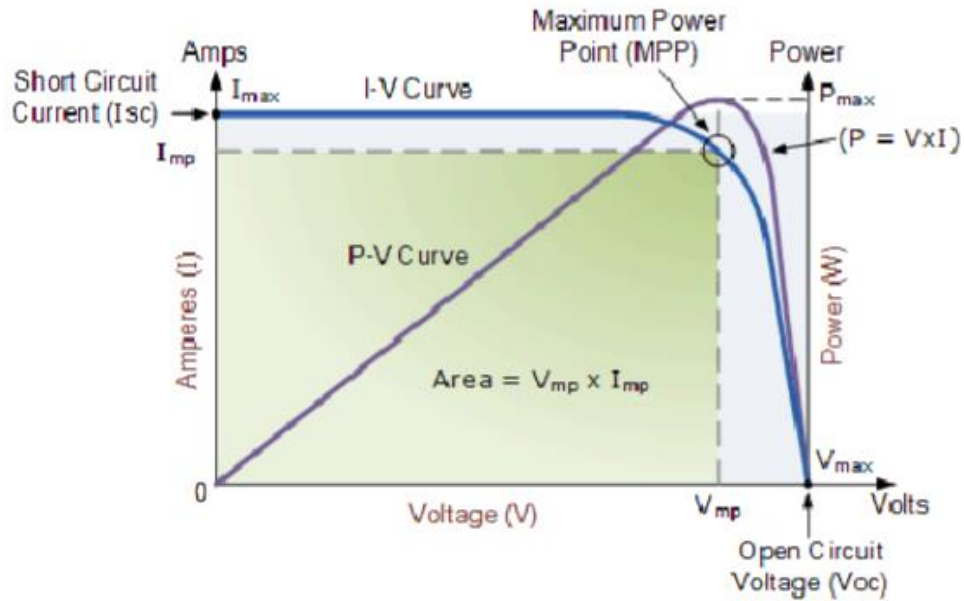


Figure 3.14. A typical I-V curve and power curve characteristics of a solar cell.

(Source: Emery, et al. 1986).

Another point of this topic is procedure. Firstly, the solar cell is connected to the devices (potentiometer and multimeter). The potentiometer set up at the minimum. The incandescent lamp is switch on and set it like that maximum area is illuminated. The distance between the solar cell and lamp should be noted. Changing the potentiometer and keeping the constant suppling voltage to the lamp, note the current and voltage via the solar cell. After it save the I-V values attaching a filter to the lamp.

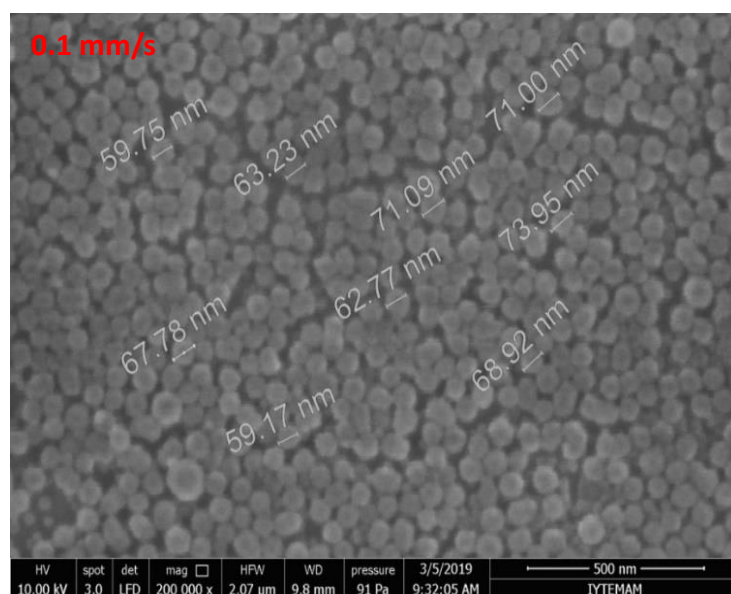
Make I-V curve of frequencies and appraise short-circuit-current (I_{SC}) without voltage. Find the value of (P_{max}) at the I-V graphic in rotation points as shown in figure and plot it how a function of dissimilar filter wavelength. Finally, by changing the lamp to sunlight repeat the procedure did above and compare the spectrum of sun and lamp with spectral reaction of Si solar cell (Source: Ramos, et al. 2010 and Villalva, et al. 2009).

CHAPTER 4

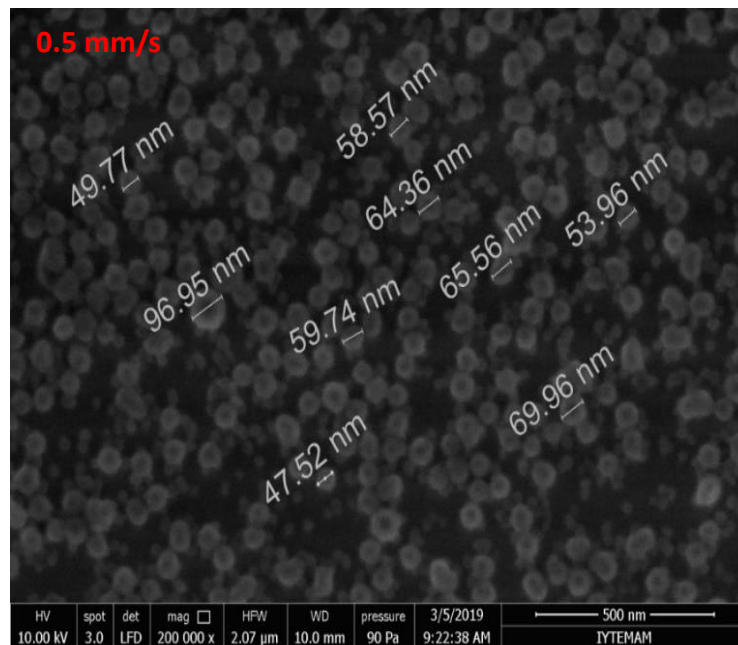
RESULTS AND DISCUSSION

4.1. SEM analysis of SiO₂ doped thin films in small area

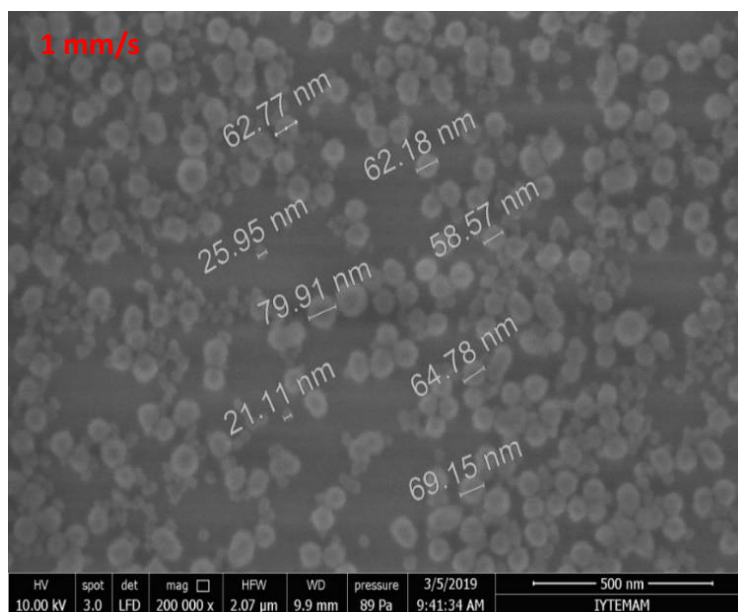
The changes surface morphology analysis of the thin films after the test was measured. The analysis for the uncoated and SiO₂ coated thin films were measured with Scanning Electron Microscope (SEM). The SEM images of the thin films deposited on SiO₂ substrate in figure 4.1(a, b c d). The films were heat-treated at 500°C after coating, but with different pulling speed from solution. As it is observed in images with changing parameter, the structure of thin films on substrate also changed. The main target in this study is to obtain 50-60 nm thickness of silica nanoparticles.



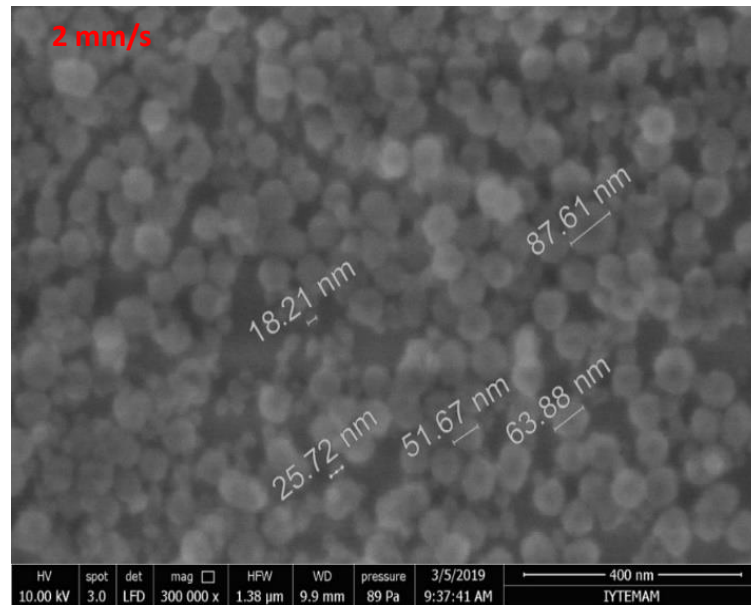
(a)



(b)



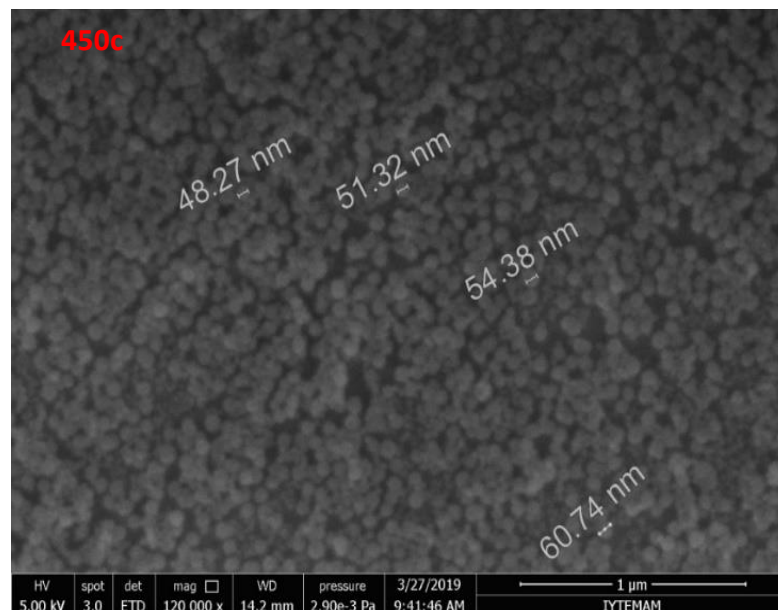
(c)



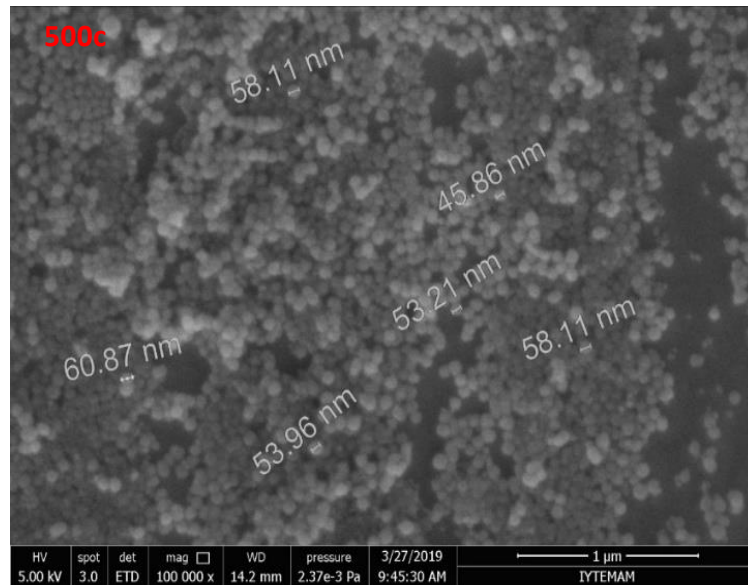
(d)

Figure 4.1(a, b, c, d) SEM analysis of SiO₂ coated thin films with different pulling speed.

At figure 4.2(a, b, c) the thin films deposited on SiO₂ substrate in another condition, 450°C-500°C-550°C (different temperature). The nanoparticles in the images are the substrate of material which belongs to soda line glass.



(a)



(b)

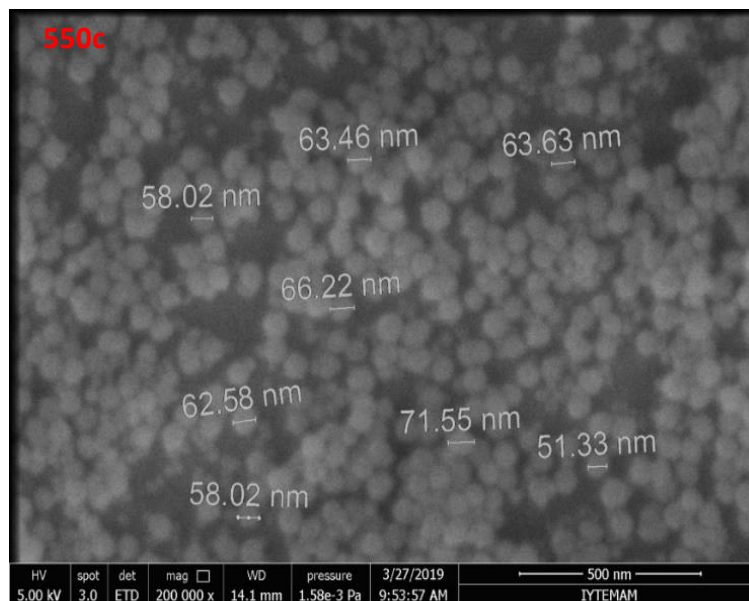


Figure 4.2(a, b, c,) SEM analysis of SiO₂ coated thin films at different temperature.

4.2. Optical characterization of small area

In this study optical characterization was explained. The changing value of transmission and reflectance analysis was obtained using spectrophotometer and proved how the nanoparticles of silicon coating effect in increasing transmission and reducing reflectance from the interface of air-glass in small area. The coated and uncoated thin-

films SiO₂ doped were measured by PerkinElmer Lambda 950 UV/VIS/NIR spectrophotometer in a wavelength between 200-2600 nm.

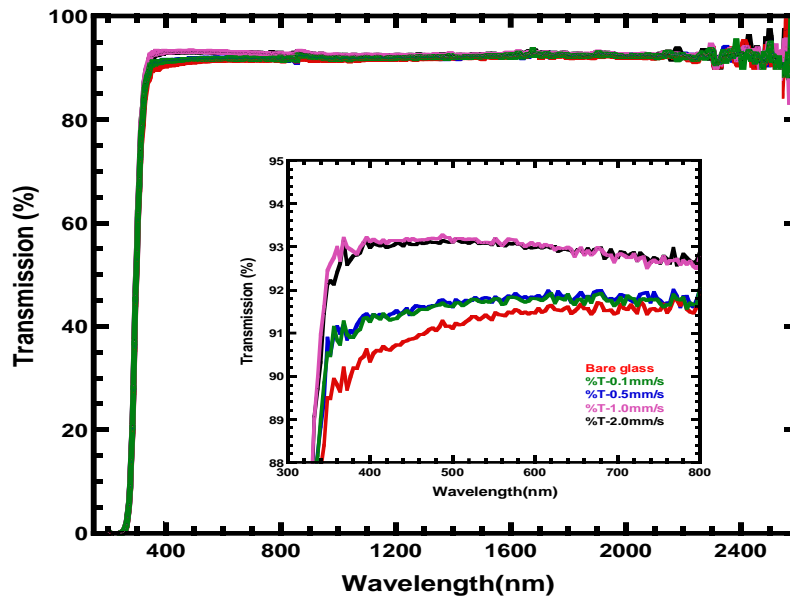


Figure 4.3. UV-spectrophotometer transmission analysis of uncoated and coated glasses with different pulling speed.

The implement optical properties of AR coatings one of the main sections in increasing performance of solar cells. According to searches and studies the thickness film with different coating speed is grown and the homogeneity is declined. In the last experiments it has been optimized. The Figure 4.3 shows the transmission across 300-700 nm range is coated and uncoated with different pulling speed at 500°C. Increasing is from 91.5% to 93.5%, as this transmittance is across 1 interface. A gain of just 2% only have been got.

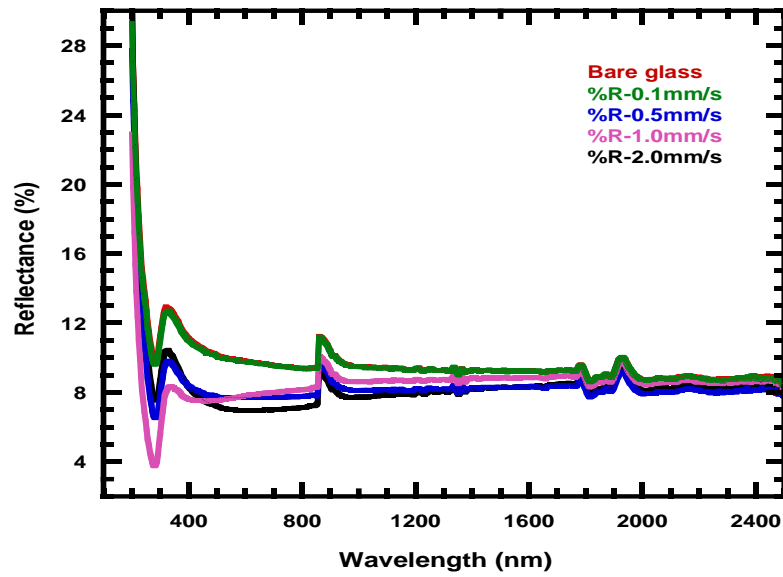


Figure 4.4. UV-spectrophotometer reflectance analysis of uncoated and coated glasses with different pulling speed.

Figure 4.4 shows the reflectance of the same study. The uncoated and coated glasses with different pulling speed at 500°C across 300-700nm. The AR coating reduced reflectance from the basic ~9% to 3.8%. This is a reflection reduction of 5.2% compared to increasing in transmission of 2%.

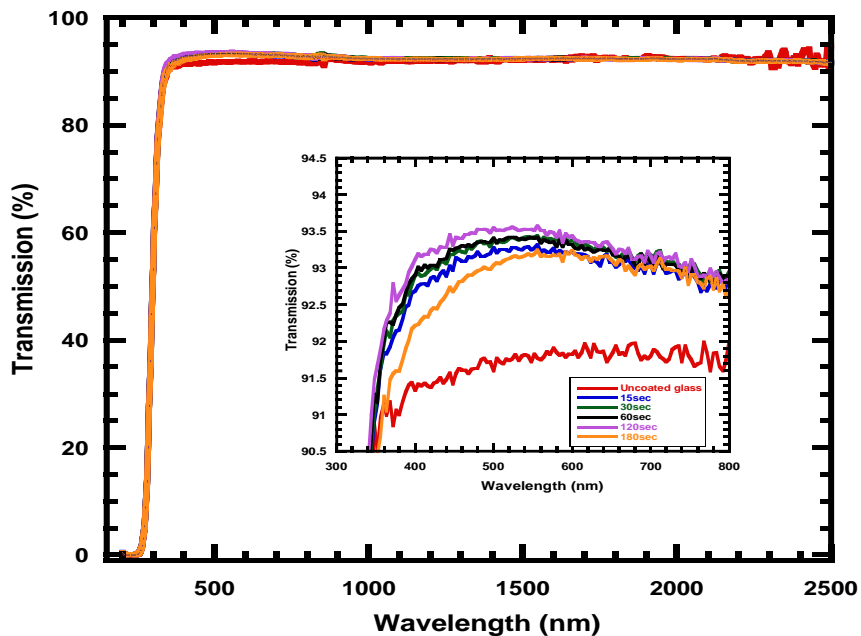


Figure 4.5(a). UV-spectrophotometer (%T) analysis with different keeping time.

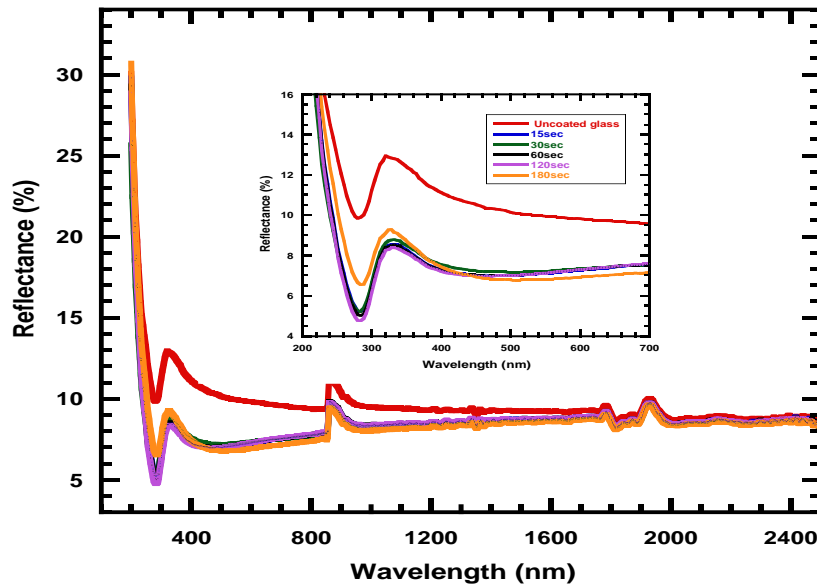


Figure 4.5(b). UV-spectrophotometer (%R) analysis with different keeping time.

Single layer coatings were deposited via dip-coating method at 500°C. The single layer coatings produce the nano-particles silicon on the surface of glasses. In the Figure 4.5(a, b) shown the result transmittance and reflectance with different keeping time in solution from 15 sec to 180 sec. As looking at 400-700nm range, the transmittance is getting more but keeping at 180 sec decreased again. The reflectance is decreasing and at 180 sec increased again. The transmission increased from 91.5% to 94% and the reflectance decreased from 9% to 4.8%. The higher result was obtained in 120 sec.

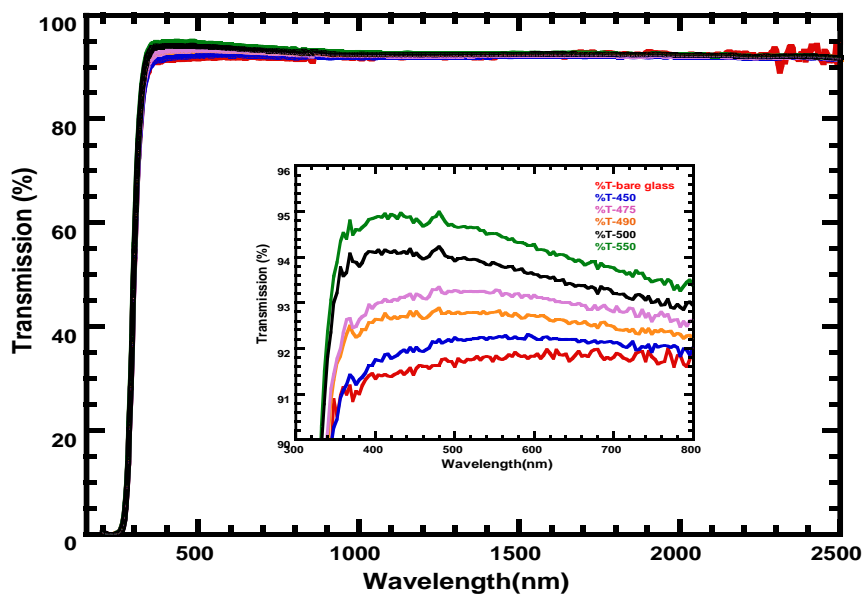


Figure 4.6(a). UV-spectrophotometer (%T) analysis with different temperature, 2.5mm/s immersion and 2 mm/sec pulling speed, 30 sec was kept on solution.

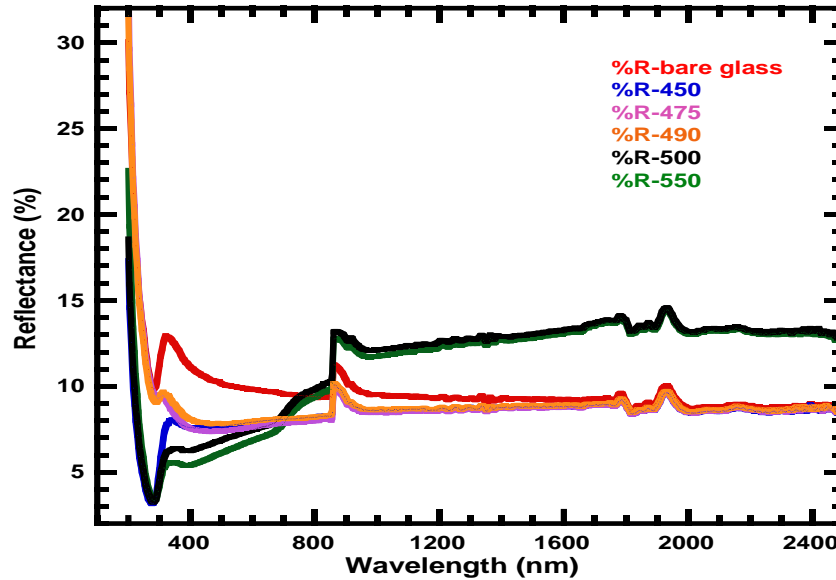


Figure 4.6(b). UV-spectrophotometer (%R) analysis with different temperature, 2.5 mm/s immersion and 2 mm/sec pulling speed, 30 sec was kept on solution.

In this study the AR coating designed to reduce reflectance and increase transmission in the wavelength range at interface glasses. But the effectiveness of single layer coating depends on how RI supporting a wavelength thickness and close to the ideal. In figure 4.6.(a) and 4.6.(b) the transmission and reflection in different temperature (450 °C to 550°C), 2.5 mm/sec immersion speed and 2 mm/sec pulling speed, 30sec was kept on solution. As shown, with increasing temperature the performance of single layer is increased too. In wavelength of 300-700nm %T has had 95%, while %R is about 3%. Compare to previous studies, a gain of just 1-2% reduction in reflectance and 1-1.5% increasing in transmittance.

4.3. Solar spectrum I-V of small area

The I-V Characteristics Curve of solar cell is a superposition of I-V-curve in the absence of darkness and when the light is available. Where the power can be extracted from diode, the I-V curve will be shifted by illumination.

There are some factors that the parameters of the source for the solar cells can be changed with temperature, incident light intensity and some factors more.

The most used parameter is efficiency, which compare the productivity of solar cells between each other. This parameter is determined as the ratio of extracted energy from solar cells to entrance energy the sun is send.

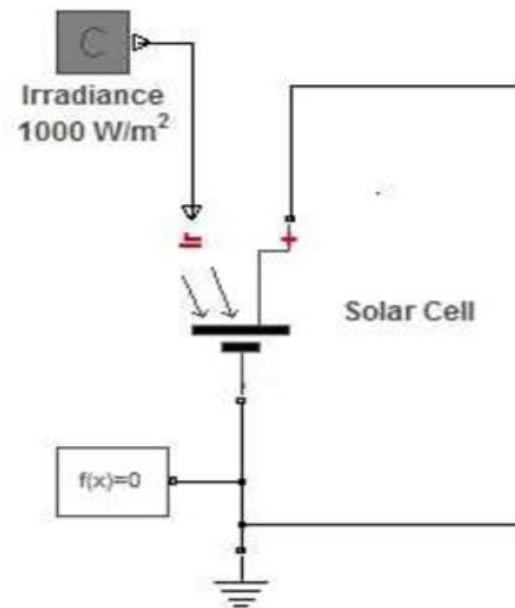


Figure 4.7. Scheme of a simple solar simulator (Source: Ramos-Hernanz, et al. 2013).

As it is observed in graphics the results in efficiency are same almost. The main goal in this research was to increase the efficiency of small and large area glasses coated solar panels and it was obtained (Source: Ramos-Hernanz, et al. 2013).

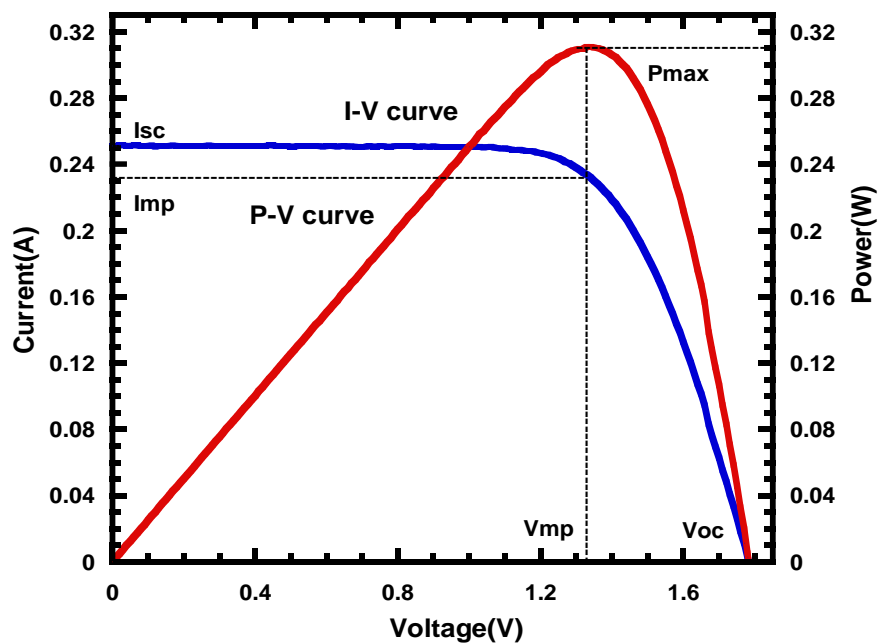


Figure 4.8. The solar cell simulator analysis of uncoated glass.

$$I_{sc} = 0.25A$$

$$V_{oc} = 1.77V$$

$$P_T = I_{sc} \times V_{oc} = 0.250A \times 1.77V = 0.44W$$

$$P_{MAX} = I_{MP} \times V_{MP} = 0.23A \times 1.31V = 0.3W$$

$$FF = \frac{Area_A}{Area_B} = \frac{I_{MP} \times V_{MP}}{I_{sc} \times V_{OC}} = \frac{0.3W}{0.44W} = 0.68$$

$$P_{MAX} = V_{oc} \times I_{sc} \times FF = 1.77V \times 0.23A \times 0.68 = 0.3W$$

$$\eta = \frac{P_{MAX}}{P_{in}} = \frac{0.3W}{2.5W} = 12.0\%$$

$$Area: 5_{CM} \times 5_{CM} = 25_{CM^2} = 0.0025m^2$$

$$Pin=1000 W/m^2 \times 0.0025m^2 = 2.5 W$$

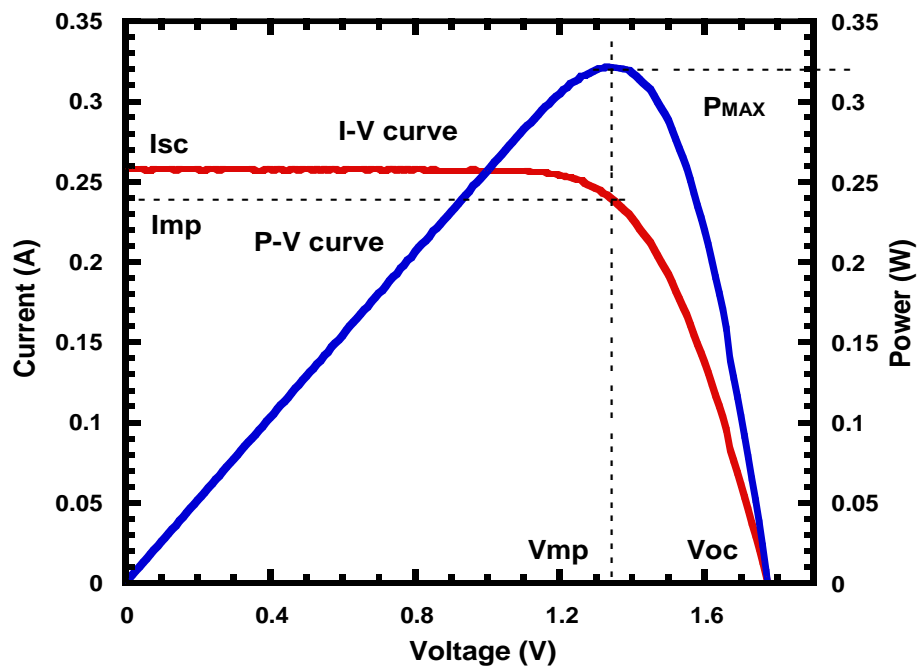


Figure 4.9. The solar simulator analysis in small are for coated glasses.

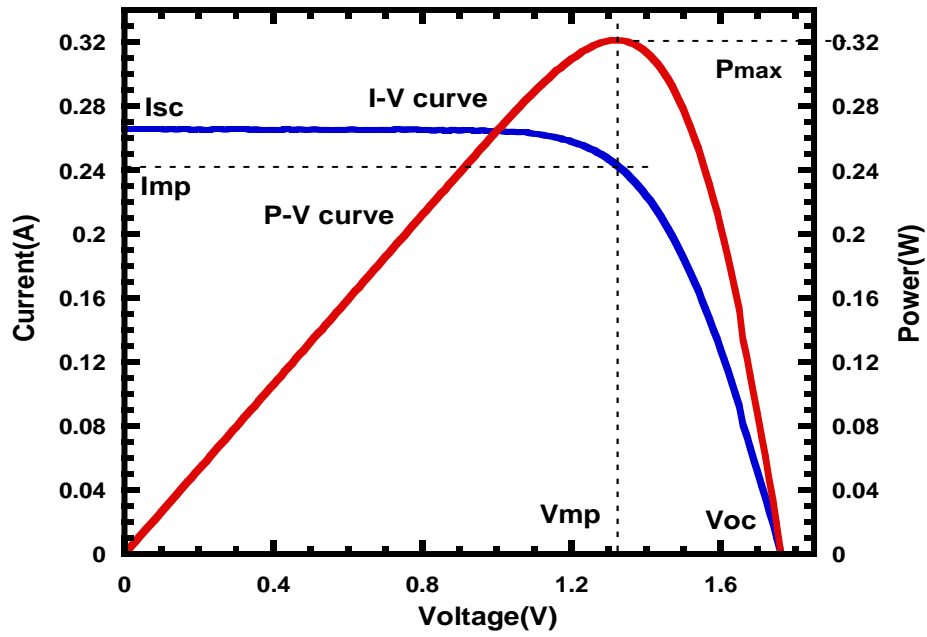


Figure 4.10. The solar simulator analysis of coated glasses in small area.

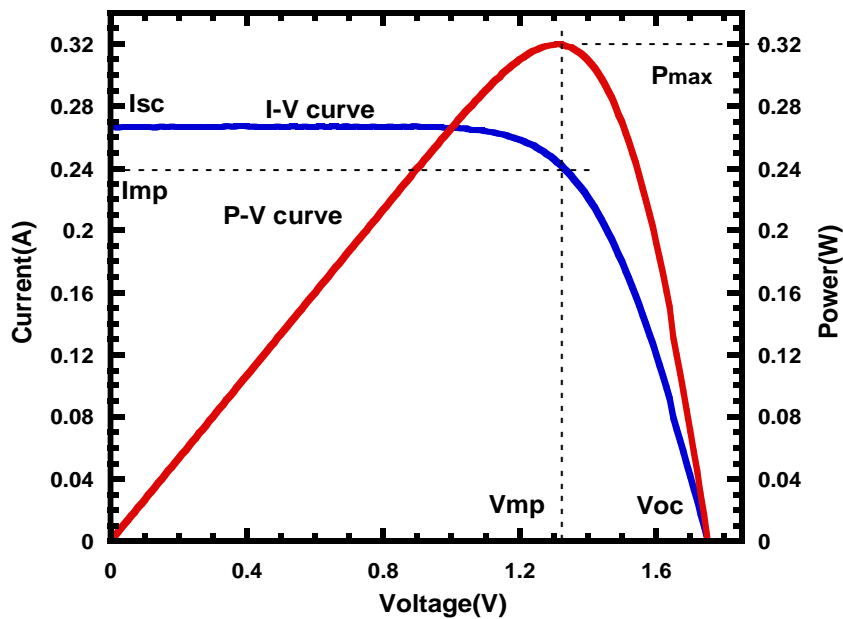


Figure 4.11. The efficiency of coated glasses in small area.

The implement thin film solar cell efficiency of coated and uncoated glasses also one of the main sections in this research. In the Figures above shown the I-V characteristics curves with blue and P-V with red color. The curves were obtained with a cell working, depending on factors of temperature and radiation. The vertical axis represents the working cell current (A) and horizontal axis the voltage (V). And this displays the amount produced energy by PV module or cell solar in the I-V curve at operating points which these axes are the operating current and voltage.

Table 4.1. The results of solar simulator analysis for coated and uncoated glasses in small area.

Small area	Efficiency	%R	%T
Figure 4.8.	12.0%	9.0%	91.0%
Cell-5x5	13.8%	-	-
Figure 4.9.	13.0%	4.5%	95.0%
Figure 4.10.	12.8%	4.5%	95.0%
Figure 4.11.	12.8%	5.0%	94.5%
Figure 4.12.	12.8%	5.0%	94.5%

In the table is placed the results of some analysis and how is it seen the values almost the same. The efficiency in uncoated glass is 12% while in coated glasses the efficiency is increased up to 12.8%-13%.

4.4. Photocatalytic Activity (MB) of small area

Investigation of photocatalytic activity using MB dye and preparation of SiO₂ thin films as a contamination procedure were reported in chapter 3. By decomposition of organic pollution cationic thiazine dye MB under UV-illumination the thin films photocatalytic activities were obtained. The maximum absorption peaks at 664 nm, 615 nm, 293 nm, and 245 nm. 664 nm is the peak that shows the Sulphur-nitrogen conjunction, but 293 nm and 245 nm show the phenothiazine forms in the MB molecules.

SiO₂ coated was prepared by dip-coating and spray-coating methods in this study. Uncoated glass, SiO₂ coated glasses were placed in the bottom of the beakers for 1, 2, 3, 4, 5 and 24 hours with 20 mL MB solution. Before starting procedure degradation, increasing intensity of absorbance value was observed by measuring MB solution as a reference. The reference value approximately 1, but not more. With Pasteur pipette 2.5 mL of solution was taken, absorbance value was measured for initial and other beakers after exposure by UV light for a time was mentioned above. Then degradation of MB was calculated as percentage.

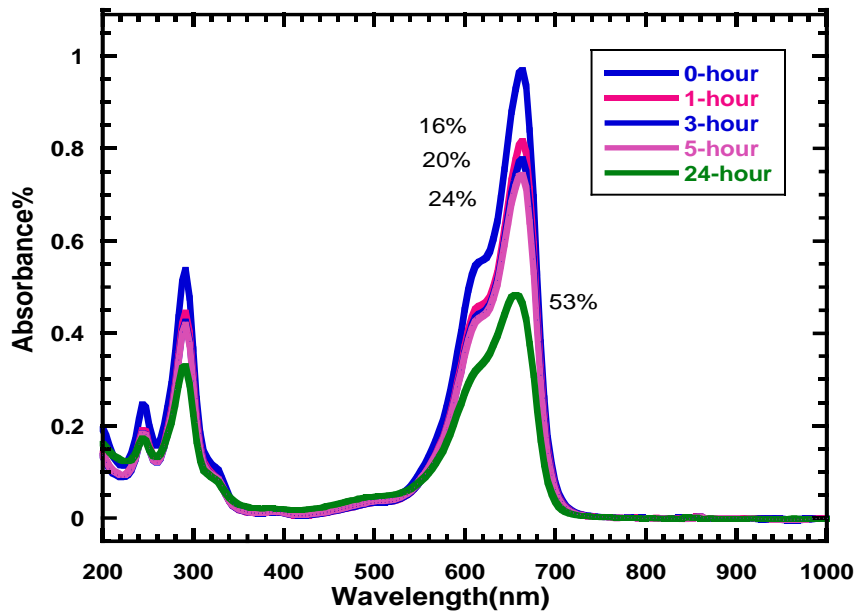


Figure 4.12. Degradation of Methylene Blue solution with bare glass.

The absorbance reduction of MB with 200-1000 nm wavelength range of various condition SiO_2 thin films degradation effect was described in Figure 4.12 to Figure 4.14.

Methylene Blue solution (20 mL) with uncoated SiO_2 thin film (3 cmx3 cm) in the bottom of the beaker was illuminated by UV source (Philips TUV 16W GJ6 T5) 20 cm away, and spectral range is 200-400 nm accordingly. The solutions were illuminated with a 1-hour interval. 664 nm is a peak absorbance value of MB that shows Sulphur-nitrogen conjugation. Changing the color of solution from dark to light blue based on this. Using uncoated SiO_2 thin film in MB solution under UV light after 1 hour 16% of MB solution was degraded, after 3 hours 20%, after 5 hours 24%, and lastly after 24 hours about 53% solution of MB was degraded. As see at Figure 4.12 in uncoated glass the value of absorbance is almost the same.

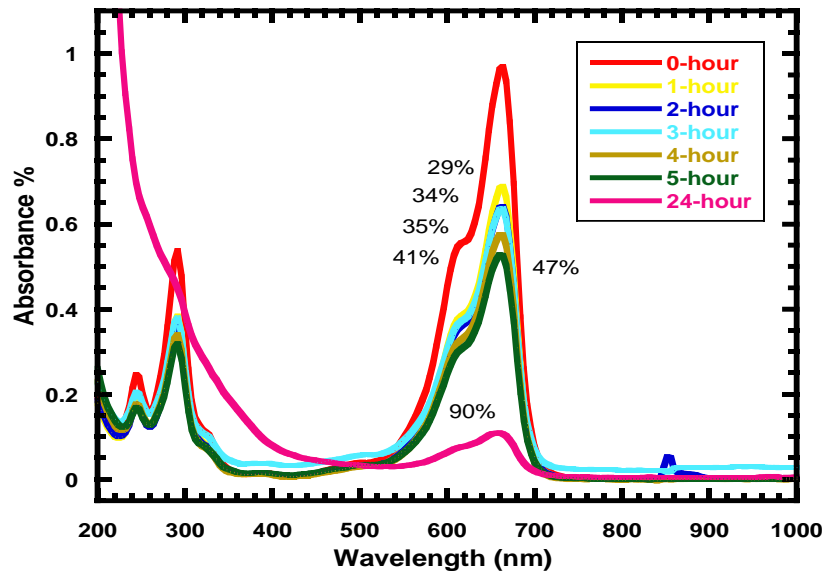


Figure 4.13. Photocatalytic degradation of Methylene Blue solution with SiO₂ coated glass (1. hours heated at 600c).

In Figure 4.13, the MB solution with coated SiO₂ thin film (coated glass was heated for 1 hour at 600°C) shown. Using coated SiO₂ thin film in MB solution under UV light after 1 hour 29% of MB solution was degraded, after 2 hours 34%, after 3hours 35%, after 4hours 41%, after 5hours 47% and lastly at 24 hours 90% was degraded as shown in Figure 4.13. By decreasing absorbance value of MB, the concentration getting lower and the colour of the solution discoloured by the time.

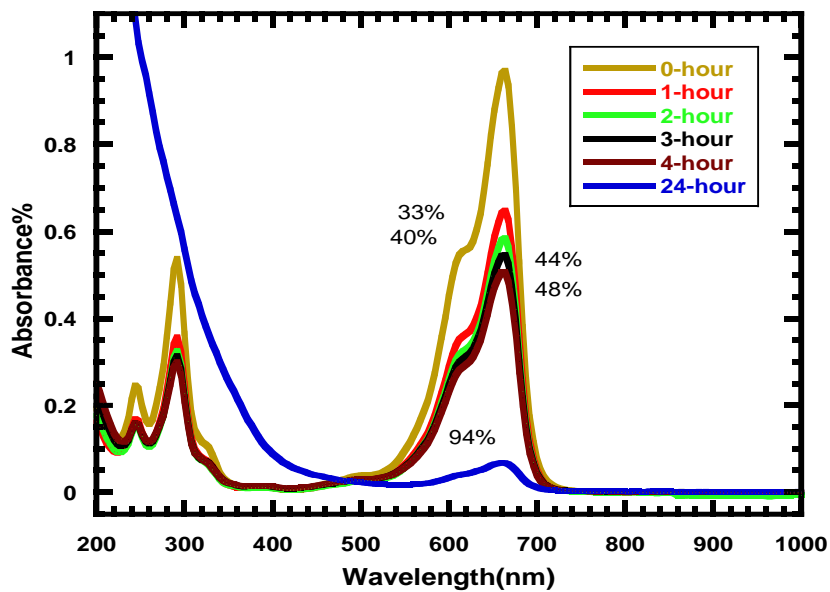
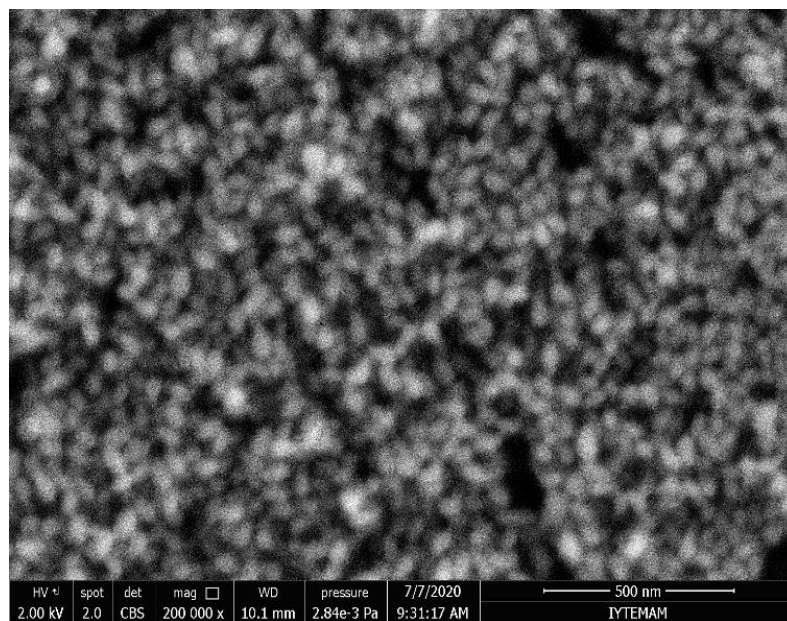


Figure 4.14. Degradation of Methylene Blue solution with SiO₂ coated glass (1. hours heated, but slow cooling).

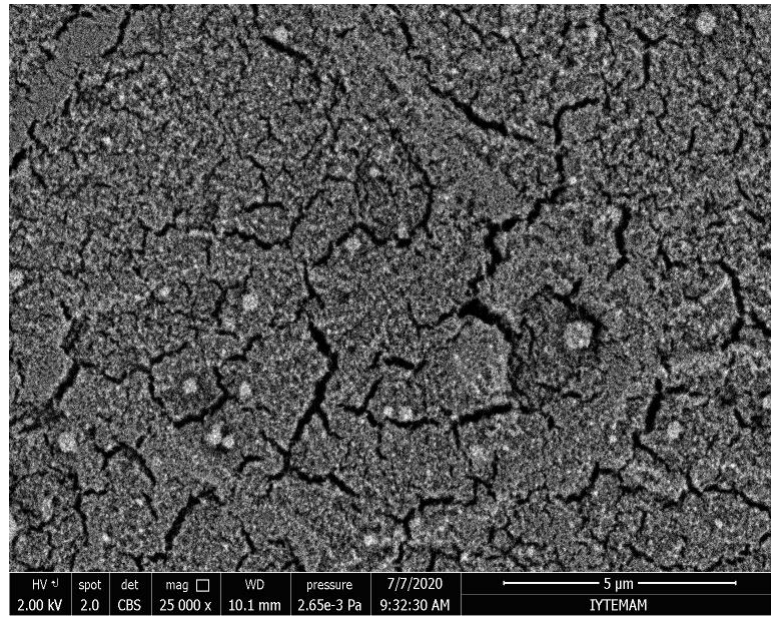
In Figure 4.14, the coated SiO₂ thin film (coating glass was heated for 1 hour, but slowly cooled). As it was mentioned above the studies were implemented by dip-coating method in small area. After keeping under UV source for 1 hour 33% of MB solution was degraded, after 2 hours 40%, 3 hours 44%, 4hours 48% and after 24 hours 94% was degraded. Compared to last result, (Figure 4.14) SiO₂ coated thin film with slow cooling at 600°C had the highest photocatalytic activity performance. By Beer Lambert Law, concentration can be calculated using absorbance values for each parts of MB.

4.5. SEM analysis of SiO₂ doped thin films in large area

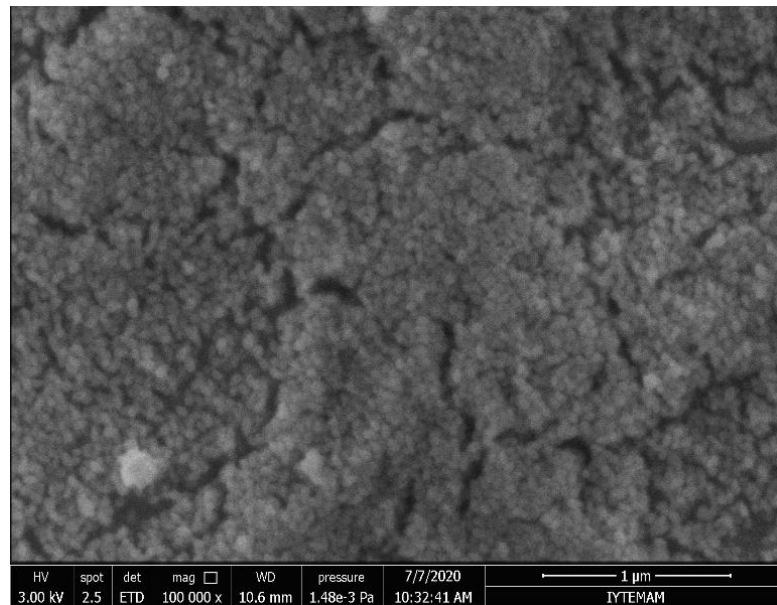
Changing surface morphology of thin film glasses in large area was shown in Figures 4.15(a, b, c). The conditions and terms were almost the same. The Scanning Electron Microscope (SEM) was used for measuring samples. The main section in this chapter was obtain 50-60 nm thickness of silica nanoparticles and it was received in large area.



(a)



(b)



(c)

Figure 4.15(a, b, c). SEM analysis of SiO₂ coated thin films at 600°C for large area.

4.6. Optical characterization of large area

In large area spray-coating was optimize. The value of %T and %R was obtained by UV-spectrophotometer in a wavelength between 200-2600nm. There are some implemented coatings below shown.

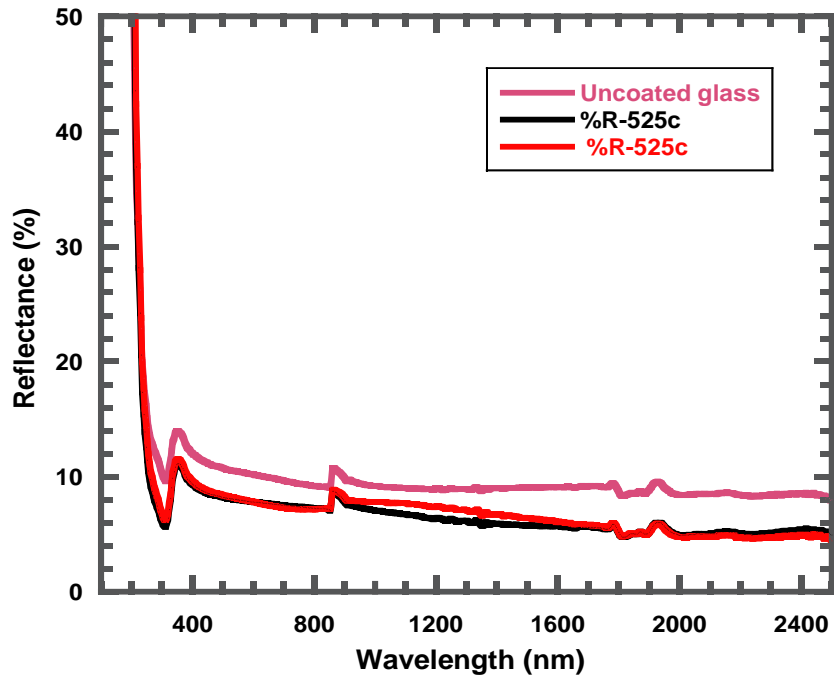


Figure 4.16. Measuring %R analysis via UV-spectrophotometer in 525°C with spray-coating deposition.

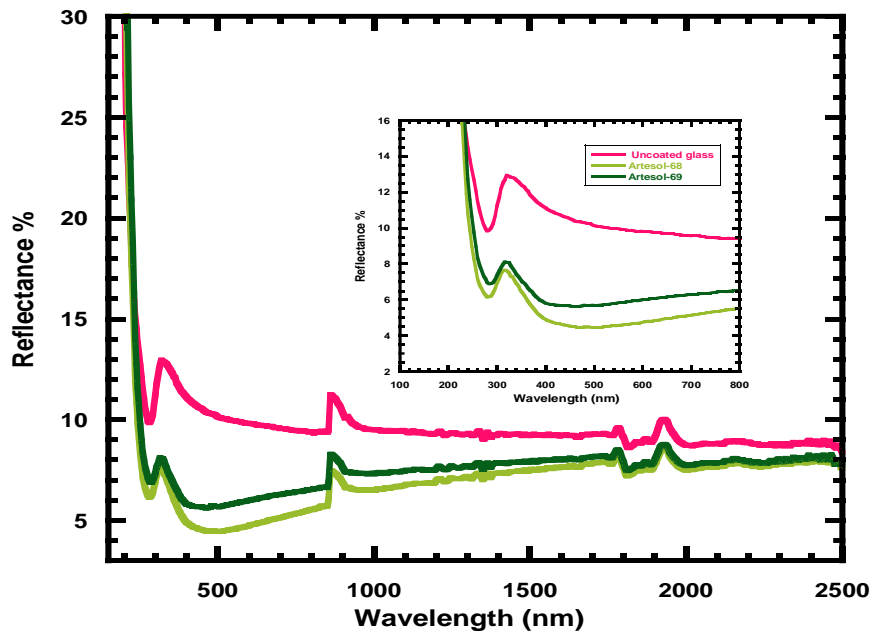


Figure 4.17(a). UV-spectrophotometer %R analysis in 600°C via spray-coating method.

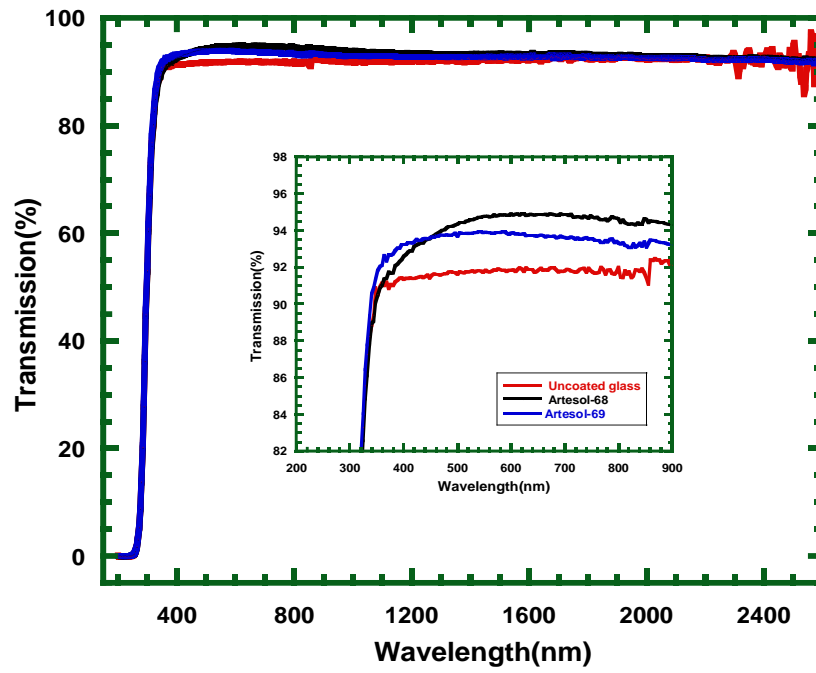


Figure 4.17(b). Measuring %T analysis via UV-spectrophotometer in 600°C with spray-coating method.

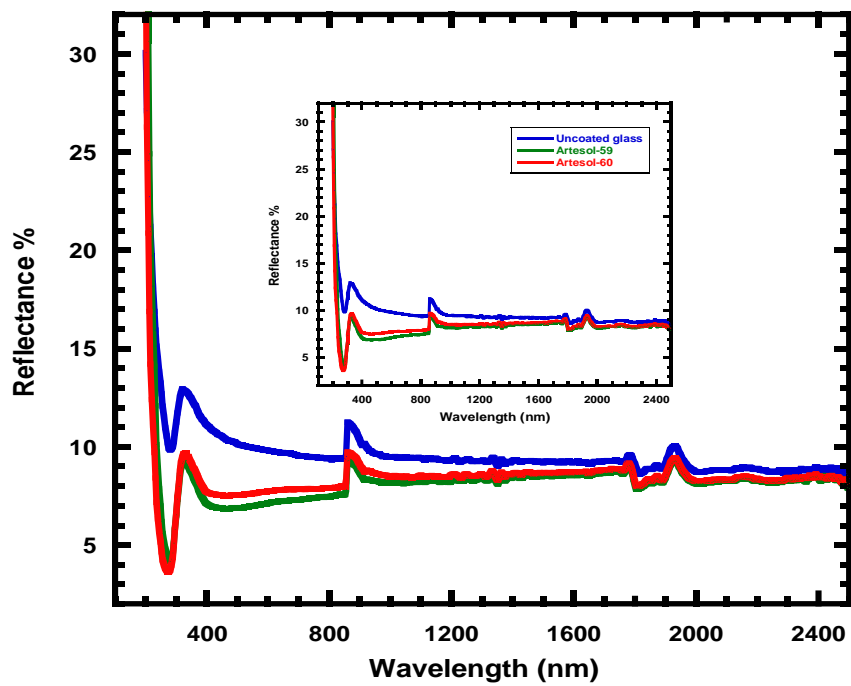


Figure 4.18(a). UV-spectrophotometer %R analysis in 600°C via spray-coating method.

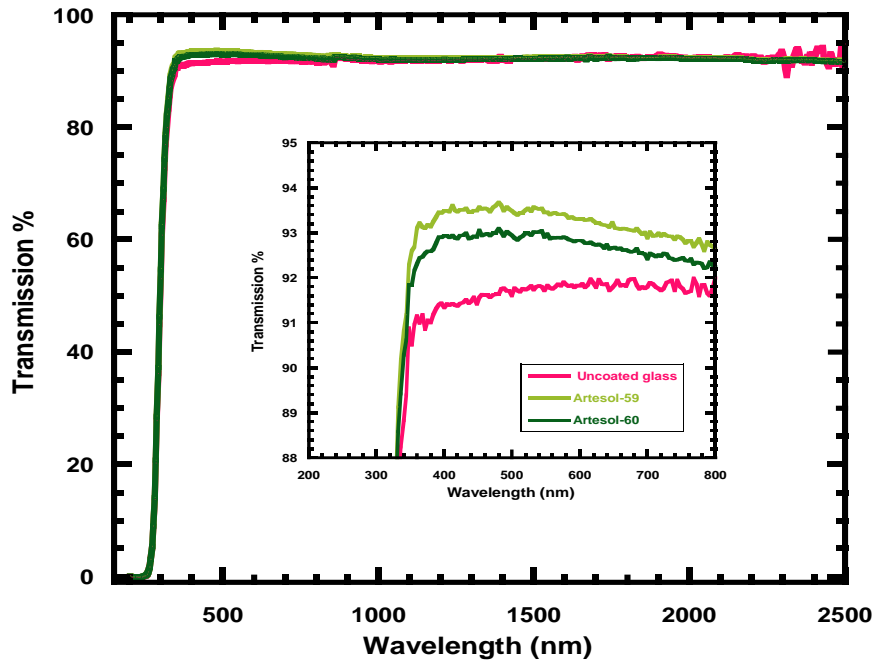


Figure 4.18(b). UV-spectrophotometer %T analysis in 600°C via spray-coating technique.

How it was mentioned above, the more increases the value of %R and %T the more increases the performance of solar cell. The coatings were optimized in different conditions in 600°C, which is shown in Table.2. In Figure 4.16 to Figure 4.18 the reflectance value changes from %6 to ~%4.2% that compared with each other, a gain of just 1.5%-1.8%. The value of %T also measured that changes from ~%92 up ~%94%.

Table 4.2. The parameters of Z(height), P(pressure) and Y(interval).

Z (cm)	P (mbar)	Y (cm)	Trials
11.0	0.1/0.8	5/4	1
12.0	0.8	3.0	2
12.5	0.6	2.0	3
12.0	0.6	2.0	4

4.7. Solar spectrum I-V of large area

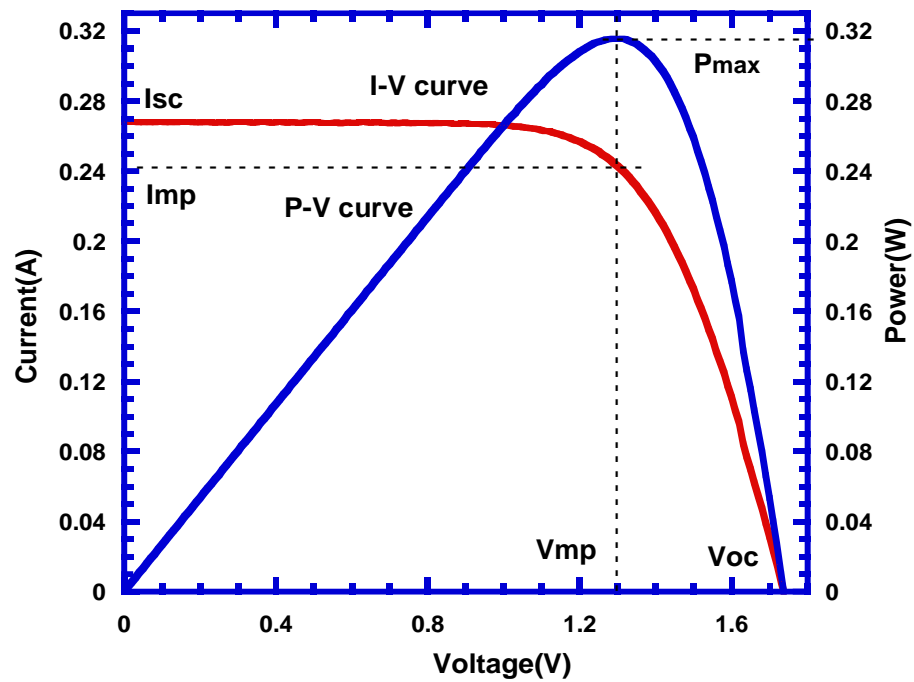


Figure 4.19. The solar simulator analysis in large are for coated glasses.

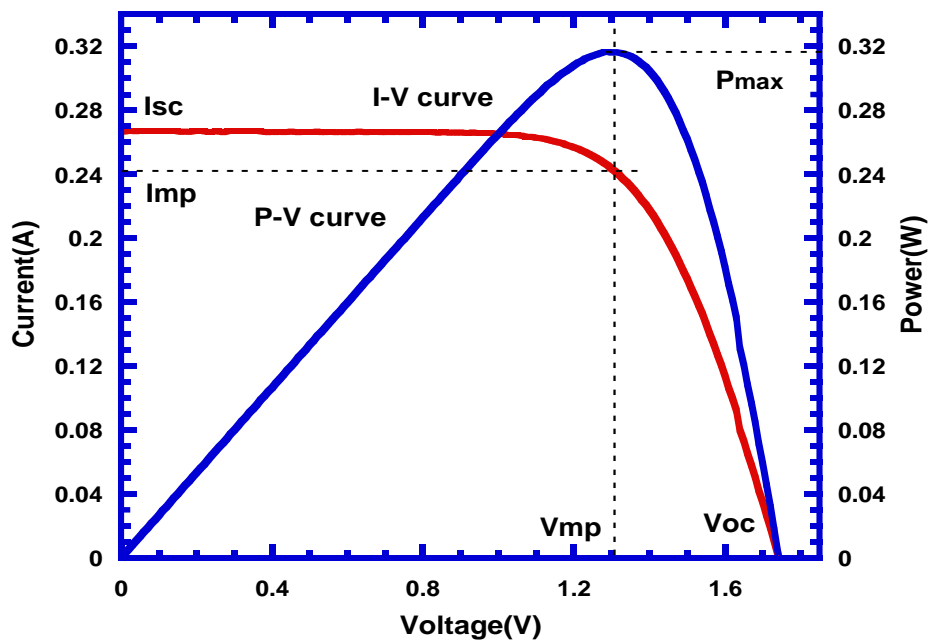


Figure 4.20. The solar simulator analysis of coated glasses in large area.

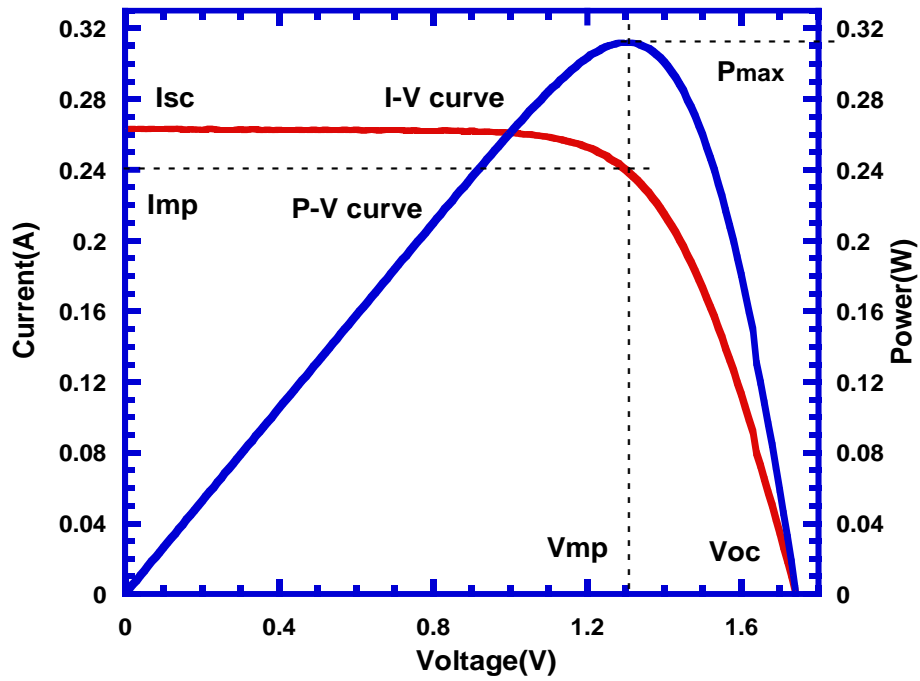


Figure 4.21. The efficiency of coated glasses in large area.

Realizing and obtaining thin film solar cell efficiency of uncoated and coated glasses in large area one of the important parts. In the Figures above shown the I-V characteristics curves with red and P-V curves with blue lines. The vertical axis represents the working cell current(A) and the horizontal axis the voltage(V). The obtained efficiencies are shown in Table 3.

Table 4.3. The results of solar simulator analysis for coated and uncoated glasses in large area.

Large Area	Efficiency	%R
Figure 4.8.	12.0%	9.0%
Cell-5x5	13.8%	-
Figure 4.19.	12.7%	6.3%
Figure 4.20.	12.7%	6.3%
Figure 4.21.	12.7%	6.3%

In the table placed the results of some analysis and how is it seen the values almost the same. The efficiency in uncoated glass is 12% while in coated glasses in large area the efficiency is increased up to 12.7%.

4.8. Photocatalytic Activity (MB) of large area

The full information was given in detail about Photocatalytic Activity (MB) in chapter 4.4. As mentioned above the studies were implemented by spray-coating method in large area. The absorbance reduction of MB with 200-1000 nm wavelength range of various condition SiO₂ thin films degradation effect in large area was characterized in Figure 4.22 to Figure 4.24.

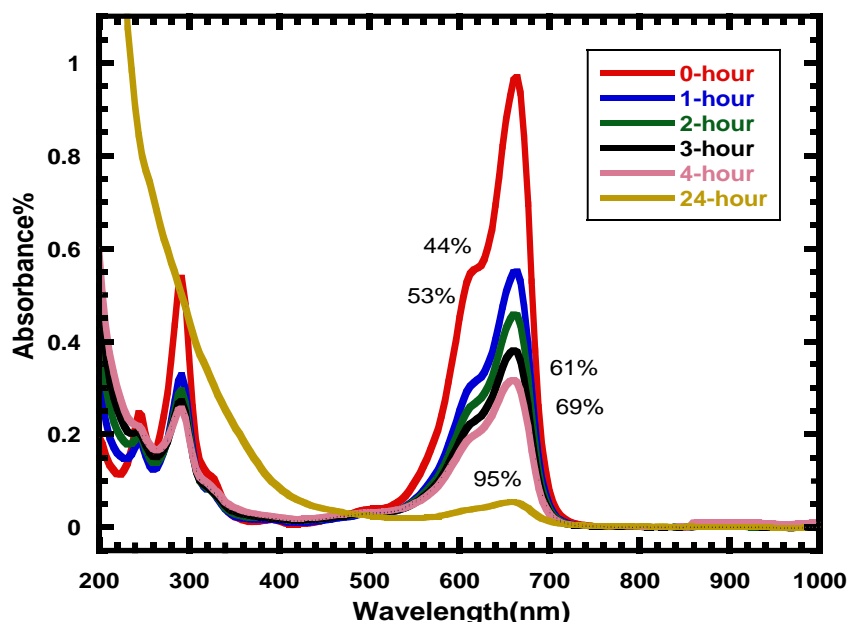


Figure 4.22. Photocatalytic degradation of MB solution with SiO₂ coated glass heated at 550 °C.

In Figure 4.22, the MB solution with coated SiO₂ thin film glass. Using coated SiO₂ thin film in MB solution under UV light after 1 hour 44% of MB solution was degraded, after 2 hours 53%, after 3hours 61.2%, after 4hours 69%, after and lastly at 24 hours 95% was degraded as shown in Figure 4.22. By decreasing absorbance value of MB, the concentration getting lower and the colour of the solution discoloured by the time.

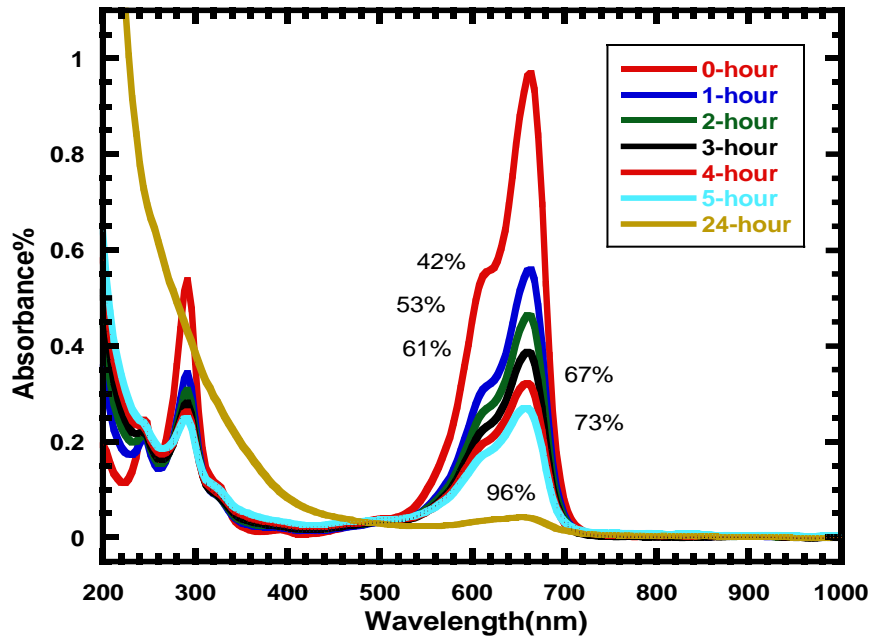


Figure 4.23. Degradation of MB solution with SiO₂ coated glass at 550 °C.

In Figure 4.23, the degradation of MB solution with coated SiO₂ thin film glass is shown. The glass was heated at 550°C for 1 hour. Using coated SiO₂ thin film in MB solution under UV light after 1 hour 42% of MB solution was degraded, after 2 hours 53%, after 3 hours 61%, after 4 hours 67%, after 5 hours 73%, after and lastly at 24 hours 96% was degraded as shown in Figure 4.23.

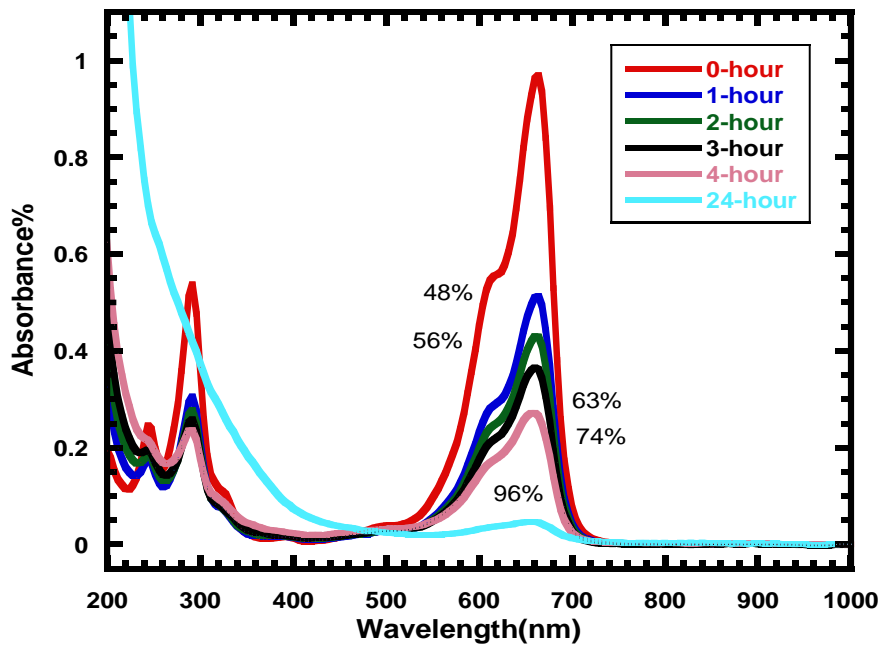


Figure 4.24. Degradation of MB solution with SiO₂ coated glass at 550 °C.

In Figure 4.24, the degradation of MB solution is shown. The temperature of heating is 550°C for 1 hour. Keeping coated glass in MB solution under UV light after 1 hour 48% of MB solution was degraded, after 2 hours 56%, after 3 hours 63%, after 5 hours 74%, after and lastly at 24 hours 96% was degraded as shown in Figure 4.24.

4.9. Durability test

In chapter 3 the adhesion test was fully described. The tape test was implemented on substrate glasses and the expected result was obtained. The substrate of glass was coated with SiO₂ nanoparticles with 50-60 nm thickness.

The main apparatus and materials for adhesion tape test are scotch, ruler, rubber eraser, illumination and sharp cutting tool. First off all before experiment the samples have to be cleaned. Through the film to the substrate between eight to eleven cuts are made, over the cuts applied the scotch and waited a while until the tape was stuck and then removed. The percentage of removed area was approximately 0-1%. The classification of adhesion test results is shown in Figures below:

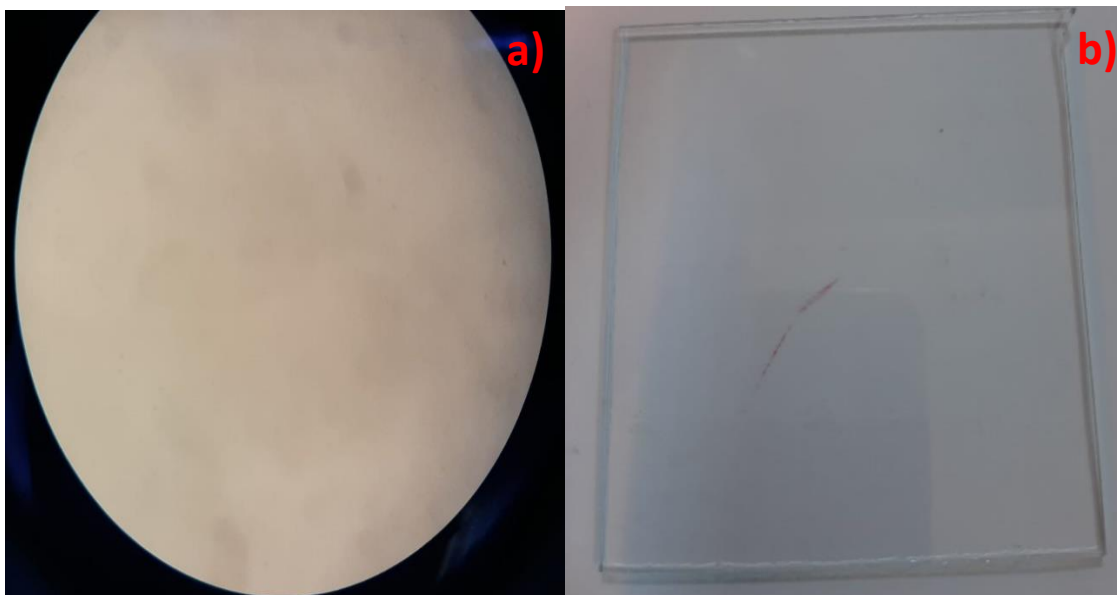


Figure 4.25. Images of uncut glass a) under microscope and b) outside the microscope.

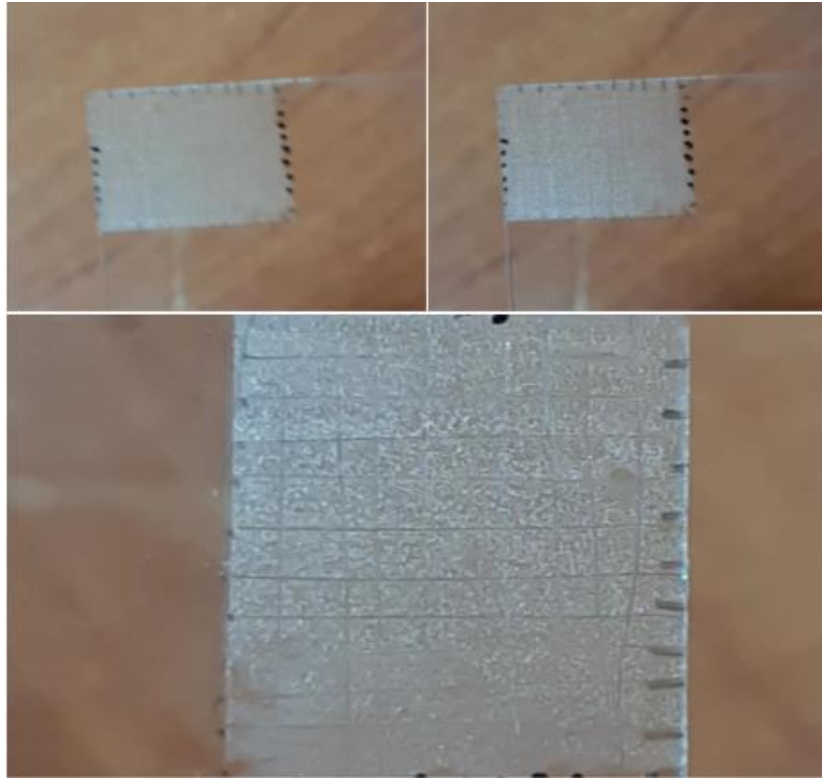


Figure 4.26. Images of cut substrate coated glass after removing scotch.

CHAPTER 5

CONCLUSION

In the last decade, a new direction has been successfully developing in the optics of thin films - the creation of antireflection coatings with the desired properties. As mentioned above one of the main purposes of research was developing optical properties of (%R-%T) in different conditions, creating the 50-60 nm thickness nanoparticles and increasing the efficiency on thin films of solar panels and comparing to uncoated surfaces. Application antireflection for thin film solar cells for provision increasing energy output is significant. Also increasing transmission and decreasing reflectance on coated substrate glass of solar technologies is one of the aspects antireflection coating. By falling the cost per (W), the efforts of solar installations in struggling global change climate is increased, therefore financial investment in ARCs is challenging. In all photovoltaic technology, the light loss into the cell approximately ~ 4.22% when it is air-glass at it. Antireflective coatings (ARC) is one of those ways to increase the efficiency of photovoltaic technologies. Through (ARC), we can achieve a decrease in the amount of reflected light at a specified interface. For deposition of thin films sol-gel techniques was used. A significant advantage of the method is the ability to easily control the composition of the material by changing the concentrations of the starting components in the solution.

The range transmission and reflectance analysis were obtained using spectrophotometer and proved how the nanoparticles of silicon coating effect in increasing transmission and reducing reflectance from the interface of air-glass in small area and large area. The coated and uncoated glasses were measured by PerkinElmer Lambda 950 UV/VIS/NIR spectrophotometer in a wavelength range 200-2600 nm. The implement optical properties of AR coatings one of the main sections in increasing performance of solar cells. According to our studies and analyses the thickness values of the AR film with different coating speed, different pulling speed and different keeping time in solution is grown and the homogeneity is declined. In the end of the analyses with counted conditions the high and increased results was obtained.

After optical characterization of AR thin films, the images of SEM analysis SiO₂ doped thin films were examined. As it was observed in SEM images the surfaces of thin films did not have a very rough structure, and also with changing the coating parameters, the structure of thin films on substrate also was changed.

Efficiency is the most used parameter, which compare the productivity of solar cells between each other. This parameter is determined as the ratio of extracted energy from solar cells to entrance energy the sun is send. The I-V characteristics curves and P-V curves were obtained with a cell working, depending on factors of temperature and radiation. The efficiency of coated glasses was determined and increased until 13% while in uncoated glass it was 12%.

Durability of thin films with tape test was assayed. Seven eight cuts were made through the film to the substrate on each direction and scotch was applied over it then removed. Under illumination was observed and removed area was not more 1%.

In photocatalytic activity, using UV-light the methylene blue solution which was an organic impurity was illuminated under device, and degradation of solution was calculated in percentage and noted.

This study has improved the understanding of antireflective and optical transparent coatings for thin film solar cells and glasses. The analysis was realized in small area with dip-coating process and large area with spray-coating technique. The results were almost similar, but there are some difference in comparison: (both sides can be coated at the same time in dip-coating but in spray-coating only one side, low waste in dip-coating high waste in spray-coating was left and others). The index of refraction was changed and thus the antireflective properties was provided.

REFERENCES

- ASTM, D. 4541 (2002) Standard test method for pull-off strength of coatings using portable adhesion testers. Philadelphia: ASTM International, 1-13.
- Augenbraun, J. J. (2010). Energy from the Sun: A Solar Feasibility Study for Macquarie University, 6-15.
- Battles, F. J., Olmo, F. J. (1995). On shadowband correction methods for diffuse irradiance measurements. *Solar Energy*, 54(2), 105-114.
- Brinker and G. W. Scherer. (1990). *Sol-Gel Science*. New York: Academic Press, 4-9.
- Brinker, C. J., & Scherer, G. W. (1990). *Sol-Gel Science: The Physics and Chemistry of Sol-Gel Processing*, Academic Press, New York.
- Chattopadhyay, S., Huang, Y. F., Jen, Y. J., Ganguly, A, (2010). Anti-reflecting and photonic nanostructures. *Materials Science and Engineering: R: Reports*, 69(1-3), 1-35.
- Chattopadhyay, S., Huang, Y. F., Jen, Y. J., Chen, K. H., & Chen, L. C. (2010). Anti-reflecting and photonic nanostructures. *Materials Science and Engineering: R: Reports*, 69(1-3), 1-35.
- Chen Fengxiang, Ai Yu, Wang Jiafu, Wang Lisheng (2010). The I-V Measurement System for Solar Cells Based on MCU, 1-5.
- Chen. (2001) "Anti-reflection coatings made by sol-gel processes: A review," *Sol. Energy Mater. Sol. Cells*, vol. 68, no. 3-4, pp. 313-336.
- Dean, J. A., Gomes, B., Bharat, K., Harik, G., & Henzinger, M. H. (2011). U.S. Patent No. 8,001,118. Washington, DC: U.S. Patent and Trademark Office, 1-13.

- DeSoto, W (2004) “Improvement and Validation of a Model for Photovoltaic Array Performance”, M.Sc. Thesis, Mechanical Engineering, University of Wisconsin, Madison, 7-17.
- Emery, Osterwald, C. (1986). Solar cell efficiency measurements. *Solar Cells*, 17(2-3), 253-274.
- Faiman, D., Feuermann, D., Ibbetson, P., Zemel, A. (1992). A multiparameter instrument for obtaining the solar beam and diffuse components, and the irradiance on inclined planes. *Solar Energy*, 48(4), 253-259.
- Fouad, O. A., Ismail, A. A., Zaki, Z. I., & Mohamed, R. M. (2006). Zinc oxide thin films prepared by thermal evaporation deposition and its photocatalytic activity. *Applied Catalysis B: Environmental*, 144-149.
- Fowles, G. R. (1989). *Introduction to modern optics*. Courier Corporation, 40-46.
- Green, M. A. (1995). *Silicon solar cells: advanced principles & practice*. Centre for Photovoltaic Devices and Systems.
- Guo, Z. Q., Liu, Y., Tang, M. Y., (2017). Super-durable closed-surface antireflection thin film by silica nanocomposites. *Solar Energy Materials and Solar Cells*, 170, 143-148.
- Handbook, (2009). *Fundamental: 2009 American Society of Heating, Refrigerating and Air-Conditioning Engineers*, 1693-1700
- Houas, A., Lachheb, H., Ksibi, M., Elaloui, E., Herrmann, J. M. (2001). Photocatalytic degradation pathway of methylene blue in water. *Applied Catalysis B: Environmental*, 31(2), 145-157.
- Kaminski, P. M., Lisco, F., & Walls, J. M. (2013). Multilayer broadband antireflective coatings for more efficient thin film CdTe solar cells. *IEEE Journal of Photovoltaics*, 4(1), 452-456.

- Kavakli, İ. G., & Kantarli, K. (2002). Single and double-layer antireflection coatings on silicon. *Turkish Journal of Physics*, 26(5), 349-354.
- Kern, W. (1970). Cleaning solution based on hydrogen peroxide for use in silicon semiconductor technology. *RCA review*, 31, 187-205.
- Kern. (1970). "Cleaning solutions based on hydrogen peroxide for use in silicon semiconductor technology," *RCA Rev.*, vol. 31, pp. 187–206.
- Lide, D, R. (1998). *Handbook of Chemistry and Physics*, 87th ed. Boca Raton, FL: CRC Press, 1-6.
- Lorente, A. Redaño, and X. De Cab. (1994) "Influence of urban aerosol on spectral solar irradiance," *J. Appl. Meteorol.*, vol. 33, pp. 406–415.
- Luque, Antonio, and Steven Hegedus. (2011). *Handbook of photovoltaic science and engineering*. John Wiley & Sons, 1-38.
- Lysko, (2014) *Measurement and Models of Solar Irradiance*, 3-18.
- Macleod and C. Clark. (2012). "Optical Coating Design with the Essential Macleod." *Thin-Film Center Inc, Tucson*, 149-151.
- Macleod, H. A. (1986). *Thin-Film Optical Filters* Hilger. Bristol, UK, 19862, 148.
- Mittal, K. L. (1978). Adhesion measurement: Recent progress, unsolved problems, and prospects. In *Adhesion measurement of thin and thick films, bulk coatings*, 1-13.
- Nelson, G. L., & Gray, K. N. *Coating Adhesion to Plastics*. (2019) In *Proceedings, Waterborne and Higher Solids Coatings Symposium (Vol. 13, pp. 5-7)*.
- Oishi, T. Ishikawa, and D. Kamoto. (1999) "Poster 2-28," in *10th International Workshop on Glass, Ceramics, Hybrids and Nanocomposites from Gels*, pp. 19–24.

- Pagliaro, M., Ciriminna, R., & Palmisano, G. (2009). Silica-based hybrid coatings. *Journal of Materials Chemistry*, 19(20), 3116-3126.
- Piebalgs, A., and J. Potocnik. (2009) "Photovoltaic Solar Energy Development and Current Research." European Communities, ISBN 978-92-79-10644 6.
- Psomopoulos, C. S., Mardikis, K. D., Katsikas, N. G., & Ioannidis, G. C. Harvesting the sun's energy in EU-27. A review, 999-1005.
- Raheem, Z. (2019). Standard Test Methods for Measuring Adhesion by Tape Test 1, 1-8.
- Ramos, J, I. Zamora, J.J. Campayo. (2010) "Modeling of Photovoltaic Module", International Conference on Renewable Energies and Power Quality (ICREPQ'10) Granada, Spain, 23-25.
- Ramos-Hernanz, J. A., Campayo, J. J., Zulueta, E., Eguía, P., & Zamora, I. (2013). Obtaining the characteristics curves of a photocell by different methods. In International Conference on Renewable Energies and Power Quality (Vol. 11, p. 1-6).
- Raut, H. K., Ganesh, V. A., Nair, A. S., & Ramakrishna, S. (2011). Anti-reflective coatings: A critical, in-depth review. *Energy & Environmental Science*, 4(10), 3779-3804.
- Riordan and R. Hulstron. (1990). "What is an air mass 1.5 spectrum?" in Conference Record of the Twenty First IEEE Photovoltaic Specialists Conference, pp. 1085–1088.
- Stackhouse, P. (2011). Surface Meteorology and Solar Energy (SSE) Data Release, p.17.
- Stocker, D. Qin, G.-K. Plattner, M. M. B. Tignor, S. K, J. Boschung, A. (2014) The Physical Science Basis." Cambridge University Press, Cambridge, UK and New York, USA, 787-801.

- Strawbridge and P. F. James. (1986). "Thin silica films prepared by dip coating," *J. Non. Cryst. Solids*, vol. 82, no. 1–3, pp. 366–372.
- Villalva, J.R. Gazoli, E. Ruppert (2009) "Modeling and Circuit Based Simulation Photovoltaic Arrays", *Brazilian Journal of Power Electronics*, Vol. 14, No.1, pp. 35-45.
- Womack, G. (2017), AR coatings and optical interference in photovoltaic (Loughborough University), 9-16, 21-23.
- Womack, G., Isbilir, K., Lisco, F., Durand, G., Taylor, A., & Walls, J. M. (2019). The performance and durability of single-layer sol-gel anti-reflection coatings applied to solar module cover glass. *Surface and Coatings Technology*, 358, 76-83.
- Wu, S. (1982). *Polymer interface and adhesion*. New York, 359-447.
- Yao, L., & He, J. (2014). Recent progress in antireflection and self-cleaning technology—From surface engineering to functional surfaces. *Progress in Materials Science*, 61, 94-143.
- Zou, Y., Gong, Y., Lin, B., and Mellott, N. P., (2016). Photodegradation of Methylene Blue in the Visible Spectrum: An Efficient W⁶⁺ Ion Doped Anatase Titania Photocatalyst via a Solvothermal Method. *Vacuum* 126: 63–69.